

Genesis of Hurricane Julia (2010) within an African Easterly Wave: Sensitivity Analyses of WRF-LETKF Ensemble Forecasts

STEFAN F. CECELSKI AND DA-LIN ZHANG

Department of Atmospheric and Oceanic Science, University of Maryland, College Park, College Park, Maryland

(Manuscript received 7 January 2014, in final form 21 April 2014)

ABSTRACT

In this study, the predictability of tropical cyclogenesis (TCG) is explored by conducting ensemble sensitivity analyses on the TCG of Hurricane Julia (2010). Using empirical orthogonal functions (EOFs), the dominant patterns of ensemble disagreements are revealed for various meteorological parameters such as mean sea level pressure (MSLP) and upper-tropospheric temperature. Using the principal components of the EOF patterns, ensemble sensitivities are generated to elucidate which mechanisms drive the parametric ensemble differences.

The dominant pattern of MSLP ensemble spread is associated with the intensity of the pre-tropical depression (pre-TD), explaining nearly half of the total variance at each respective time. Similar modes of variance are found for the low-level absolute vorticity, though the patterns explain substantially less variance. Additionally, the largest modes of variability associated with upper-level temperature anomalies closely resemble the patterns of MSLP variance, suggesting interconnectedness between the two parameters. Sensitivity analyses at both the pre-TD and TCG stages reveal that the MSLP disturbance is strongly correlated to upper-tropospheric temperature and, to a lesser degree, surface latent heat flux anomalies. Further sensitivity analyses uncover a statistically significant correlation between upper-tropospheric temperature and convective anomalies, consistent with the notion that deep convection is important for augmenting the upper-tropospheric warmth during TCG. Overall, the ensemble forecast differences for the TCG of Julia are strongly related to the processes responsible for MSLP falls and low-level cyclonic vorticity growth, including the growth of upper-tropospheric warming and persistent deep convection.

1. Introduction

Although tropical cyclogenesis (TCG) has been a main focus of numerous modeling studies and observational campaigns in recent years, the formation of tropical depressions (TDs) and their evolution into tropical storms (TSs) remain poorly understood. The process by which a nondeveloping tropical disturbance intensifies into a TS-like system involves multiple scales of interactive processes, ranging from cloud microphysics to meso- γ - and synoptic-scale motions. Theories to describe the formation of a low-level meso- β -scale vortex (LLV) within an African easterly wave (AEW) have attempted to paint a complete picture of TCG within an easterly wave in the northern Atlantic and eastern Pacific basins. There still are, however, many unanswered questions regarding the

dynamical and thermodynamical transitions taking place during TCG because of the lack of high-resolution spatial and temporal data.

Cloud-permitting models have been used to provide novel insights into the development of some non-observable features of TCG, such as convective bursts (CBs) and meso- γ -scale vortices (Cecelski and Zhang 2013, hereafter CZ). Additionally, numerous studies have investigated the theories created to describe the roles of the AEW during TCG in addition to the formation of the LLV. The AEW has recently been thought of as the parent to the LLV under the marsupial pouch paradigm (Dunkerton et al. 2009; Wang et al. 2010; Montgomery et al. 2010), with both observational studies (Montgomery et al. 2012; Braun et al. 2013) and high-resolution modeling studies having demonstrated its usefulness. When the AEW is thought of in this manner, the growth of the LLV is presumed to take place from the bottom up, resulting from the formation and aggregation of vortical hot towers (VHTs) and other mesovortices (Hendricks et al. 2004; Montgomery et al.

Corresponding author address: Dr. Da-Lin Zhang, Department of Atmospheric and Oceanic Science, University of Maryland, College Park, College Park, MD 20742.
E-mail: dalin@atmos.umd.edu

2006; CZ). The existence of VHTs, mesovortices, and their aggregation have been shown in observational and modeling studies, supporting the notion that they are the “building blocks of TCG” (Sippel et al. 2006; Houze et al. 2009; CZ). More recently, upper-tropospheric thermodynamic changes have been shown to induce meso- α -scale mean sea level pressure (MSLP) falls during TCG (Zhang and Zhu 2012; CZ), further supplementing the marsupial pouch paradigm and the formation of the LLV. The MSLP falls aid the development of the LLV via enhanced planetary boundary layer (PBL) convergence near the AEW pouch center (CZ). This warming aloft is not considered to be resultant from balanced flow but instead by an imbalance of latent heating due to the depositional growth of ice in the upper troposphere (CZ).

A more innovative way to investigate the dynamics and thermodynamics of TCG is through ensemble simulations, though its use has just begun. By perturbing the initial conditions (ICs) of an individual model, a suite of forecasts can be generated for the TCG of a particular storm. Two notable studies have used a single model ensemble to investigate TCG: Sippel and Zhang (2008) and Cecelski et al. (2014, hereafter CZM). The former used short-range fifth-generation Pennsylvania State University–National Center for Atmospheric Research Mesoscale Model (MM5) ensemble forecasts to investigate a nondeveloping disturbance in the Gulf of Mexico and concluded that the presence of a moist tropospheric column and high convective available potential energy (CAPE) are the two most important ICs for TCG. The higher CAPE and greater column moisture content enables a faster spinup in some ensemble members, which, in turn, undergo TCG faster. The latter uses the Weather Research and Forecasting–local ensemble transform Kalman filter coupled system (WRF-LETKF; Hunt et al. 2007; Miyoshi and Kunii 2012) to generate twenty 1-km-resolution ensemble forecasts for the TCG of Hurricane Julia (2010). Their work showed that the differences in TCG between the ensemble members was related to convective initiation early in the simulations in addition to the creation of a storm-scale outflow and upper-tropospheric warming during TCG.

While CZM studied differences between developing and nondeveloping members from the WRF-LETKF ensemble forecasts, a statistical approach to making inferences on the dynamics and thermodynamics (e.g., MSLP changes) of TCG can provide a more holistic view of the ensemble forecasts. Sippel and Zhang (2008) employed a linear correlation analysis, following Hawblitzel et al. (2007), to generate statistical sensitivities of MSLP changes and isolated variables that are responsible dynamically for the changes. More recently, studies have

used ensemble sensitivity analyses (Chang et al. 2013; Zheng et al. 2013; Gombos et al. 2012; Torn and Hakim 2008; Ancell and Hakim 2007) to examine how a particular forecast metric depends on ICs. Ensemble sensitivity uses a linear correlation between a chosen forecast metric and selected meteorological parameters to generate a statistical sensitivity of the forecast metric for previous forecast times and the ICs. Instead of using just an individual ensemble member, the analysis is able to use all ensemble members, yielding the ability to make inferences about what meteorological parameters the whole complement of ensemble forecasts are sensitive to. Ensemble sensitivity has been shown to be useful in short- and medium-range forecasts for midlatitude applications (Chang et al. 2013; Zheng et al. 2013), as well as TC track forecasts (Gombos et al. 2012), even with the assumption of linearity. The selection of a forecast metric has varied across previous studies, ranging from selecting particular cyclone parameters (e.g., MSLP) to the principal components (PCs) of empirical orthogonal functions (EOFs), whose use has produced promising results (Chang et al. 2013; Zheng et al. 2013; Gombos et al. 2012). Recently, the use of ensemble sensitivity analyses via EOFs was extended by Torn and Cook (2013) for two TCG cases from the 2010 North Atlantic hurricane season. Their results depicted that the forecasts of TCG were sensitive to select, but different, parameters. The first storm investigated, Hurricane Danielle, was most sensitive to upper-level divergence and deep-layer (e.g., 850–200 hPa) vertical wind shear (VWS). In contrast, the second storm, Hurricane Karl, was more sensitive to a coherent large-scale vortex structure in addition to a weaker sensitivity to the magnitude of VWS. Such differences between two storms in the same hurricane season depict the complexity in understanding TCG and related processes across all space and time scales.

In this study, we discuss the results of ensemble sensitivity analyses for the TCG of Hurricane Julia from the 2010 North Atlantic hurricane season. Using 20 high-resolution ensemble forecasts generated by WRF-LETKF (see CZM), this study focuses on understanding the disagreements between the ensemble members for several parameters such as MSLP, the upper-tropospheric outflow layer, and deep convection. Using a series of EOFs, the parametric patterns of ensemble variance can be identified, and sensitivity analyses are performed to provide statistical inferences about which meteorological processes might be responsible for these differences. Thus, the objectives of this paper are (i) to identify the dominant ensemble forecast patterns for disagreement of MSLP and low-level absolute vorticity; (ii) to discern which processes are responsible for the MSLP differences, with a focus on

upper-tropospheric thermodynamic changes per our previous findings; (iii) to pull out the dominant modes of ensemble variance for upper-tropospheric thermal anomalies and diagnose the sensitivity of this variance to the upper-tropospheric divergent outflow layer and deep convection; and (iv) to investigate the ensemble variability of deep convection.

The next section provides an overview of Hurricane Julia. Section 3 describes the ensemble sensitivity methodology and model data used. Sections 4 and 5 present the dominant ensemble forecast differences for the pre-TD and TD stages, respectively.

2. Overview

Before elaborating on the ensemble sensitivity analysis, it is desirable to briefly summarize some pertinent information about Hurricane Julia. The storm was declared a TD by the National Hurricane Center (NHC) at 0600 UTC 12 September (12/0600), quickly becoming a TS 12 h later. Julia developed within a potent AEW with the MSLP disturbance evolving from a meso- β -scale feature induced by pronounced upper-tropospheric warming (CZ). The LLV resulted from bottom-up growth of cyclonic vorticity and the merging of two main mesovortices in a meso- β region characterized by enhanced PBL convergence during the hours prior to 12/0600. As shown in CZ, the evolution of the tropical disturbance into a TD predominately took place between 12/0000 and 12/0600, with initial signs of a mesoscale MSLP disturbance noticeable at 11/1800.

CZM have described the full methodology of how the 20 ensemble forecasts were created. Briefly, the 20 perturbed ICs are created by integrating WRF-LETKF (Miyoshi and Kunii 2012) for 96 h from 05/0000 to 10/0000, terminating at the initialization time of the control simulation from CZ. A 27-km-resolution domain was utilized for the WRF-LETKF process (“LETKF”; Fig. 1a) and employed observational data from the Global Data Assimilation System (GDAS) hosted by the National Centers for Environmental Prediction (NCEP). Using these perturbed ICs, the 20 ensemble forecasts were created using the same domain setup as the control (Fig. 1a), but with the addition of the LETKF domain to supply lateral and initial conditions to the inner domains D1, D2, and D3, whose horizontal resolutions are 9, 3, and 1 km, respectively. These 20 ensemble forecasts were integrated for a total of 66 h from 10/0000 to 12/1800, consistent with the control simulation described in CZ, terminating at the time Julia was declared a TS. The ensemble forecasts utilized the same parameterization schemes as the control, while the lateral boundary conditions for the outermost (LETKF) domain were

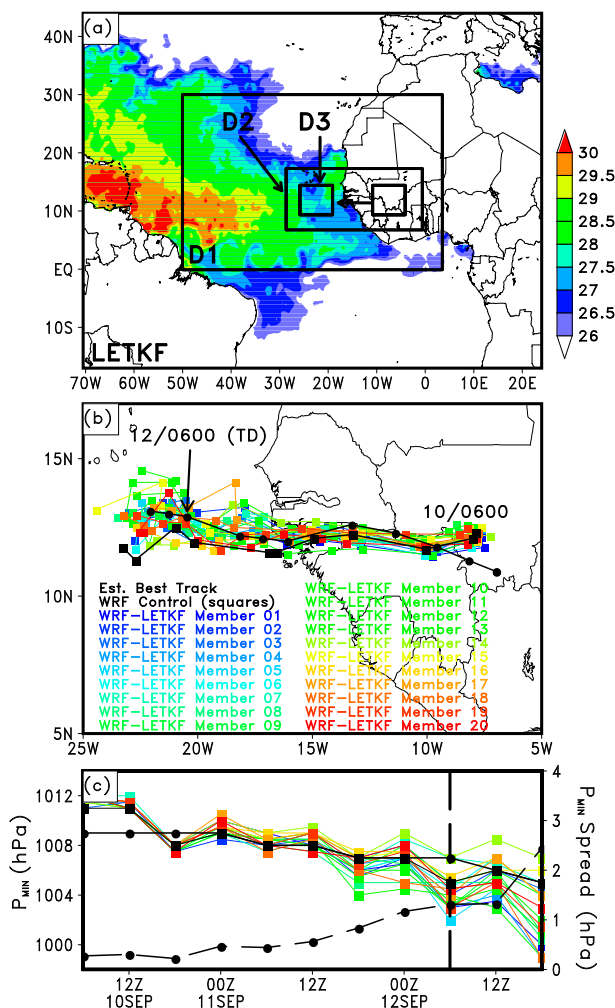


FIG. 1. (a) Domain setup of the ensemble forecasts overlaid with National Oceanic and Atmospheric Administration (NOAA) Optimal Interpolation sea surface temperatures at 0000 UTC 10 Sep 2010. The domains LETKF, D1, D2, and D3 represent 27-, 9-, 3-, and 1-km-horizontal-resolution domains, respectively. The 1-km domain is a moving domain with its starting and final position depicted. Comparisons of the 20 WRF-LETKF ensemble forecasts (differentiated by colors) for (b) storm track and (c) storm intensity in terms of minimum central pressure, with NHC best estimates in black circles, and the control simulation in black with squares. The ensemble spread for P_{MIN} is shown by the dashed line in (c) while the vertical dashed line represents 0600 UTC 12 Sep, the time that Julia was declared a TD by NHC.

supplied by the European Centre for Medium-Range Weather Forecasts Interim Re-Analysis (ERA-Interim). For further descriptions of the WRF parameterizations utilized or the ensemble methodology, readers are encouraged to see CZ and CZM.

Utilizing the ensemble forecasts generated as described above, CZM conducted a parametric investigation of the ensemble forecasts for the TCG of Julia. The

method involved selecting, comparing, and contrasting faster-developing members with nondeveloping members for a variety of parameters such as upper-tropospheric warming, convective initiation near the AEW pouch center, and characteristics of the upper-level outflow layer. Out of the 20 members, 3 members were used in the study in addition to the control simulation: a fast developer, a nondeveloper, and an ensemble member whose MSLP disturbance best represented the estimates by the NHC. Additionally, CZM alluded to trends in the full ensemble by demonstrating a strong linear correlation between area-averaged upper-tropospheric temperatures and MSLP at 12/0000 and 12/0600.

While CZM provided meaningful results from utilizing only four simulations, the study herein focuses on expanding the investigation beyond a handful of ensemble members. To this end, we investigate here the ensemble forecast disagreements associated with TCG by utilizing the whole complement of ensemble members (i.e., 20 members) to describe the major ensemble differences for the development of Hurricane Julia. Furthermore, we attempt to identify what mechanisms might be responsible for these differences. Figures 1b and 1c show the simulated tracks and intensity from each ensemble member. Focusing on the storm intensity as described by central minimum pressure P_{MIN} , it is evident that the ensemble spread (e.g., disagreements from the ensemble mean) nears 1 hPa at 11/1800 and surpasses 1 hPa by 12/0000 and 12/0600 (Fig. 1c). While not completely evident from the P_{MIN} analysis, some ensemble simulations undergo TCG prior to 12/0600, while others never develop a TD. In particular, CZM noted that two main ensemble members never develop while there was a large ensemble bias for storms stronger than what was estimated by NHC (Fig. 1c). Thus, it was concluded that the TCG of Hurricane Julia was highly predictable, though the seemingly small spread in P_{MIN} yielded significant ensemble member differences dynamically. Noting the various ensemble solutions and their differences, we can use EOF analyses and ensemble sensitivities to pull out dominant patterns of ensemble disagreements and the mechanisms possibly that are responsible for such disagreements.

3. Methodology

The ensemble sensitivity analyses performed herein employ EOFs and related PCs as forecast metrics, following those used by Chang et al. (2013) and Zheng et al. (2013). Typically, EOFs are created in temporal and spatial dimensions, with the PCs representing the time series of the EOF pattern. Alternatively, we calculate EOFs using the ensemble dimension in lieu of the time

dimension. Essentially, anywhere the time dimension is used is replaced with the ensemble dimension in the EOF calculation, ranging from 1 to M , where $M = 20$ (i.e., the number of ensemble members). Thus, the 20 values of a PC (referred to as ‘‘PC values’’) represent how strongly a particular ensemble member projects on to the particular phase of the related spatial EOF pattern. We generate EOFs at two important stages in the evolution of Julia: (i) pre-TD: 11/1800 and 12/0000 and (ii) TD: 12/0600. These times are chosen based on the emergence of MSLP disturbances in some faster-developing members in addition to being times when the ensemble spread nears or exceeds 1 hPa (Fig. 1c). These times correspond to 42-, 48-, and 54-h integration times from the ensemble forecasts. We create the EOFs over a 10° longitude \times 6° latitude domain encapsulating the storm centers of each ensemble member at each respective time using simulation data from the 27-km-resolution domain. The sensitivity analyses will focus on the PCs from one of the two leading EOF patterns, as these explain the largest portion of the total variance of the respective parameter, while the third and beyond EOFs explain substantially less total variance (typically less than 10% for the respective parameter).

While assessing these EOF patterns, care needs to be taken in understanding their physical significance. The EOF spatial pattern carries the same unit as the forecast variable (e.g., hectopascals for MSLP) with the amplitude representing the amount of the ensemble sample standard deviation explained by the EOF. The sign of the pattern does not matter, but the spatial characteristics of the pattern do have physical significance. That is, the spatial patterns of the EOFs can represent intensity and position differences of a cyclone (Chang et al. 2013; Zheng et al. 2013; Gombos et al. 2012), which, for our use, will be the intensity and position ensemble differences of the pre-TD and TD phases of Julia. Since TCG denotes the transition of a nondeveloping tropical disturbance into a developing one, the PC of the EOF pattern representing an intensity disagreement is used preferentially in the sensitivity analyses.

As previously mentioned, the PC of either the leading EOF pattern (EOF 1) or second EOF pattern (EOF 2) will act as a forecast metric for our sensitivities. Following Chang et al. (2013) and Zheng et al. (2013), ensemble sensitivity is defined as

$$\text{Sensitivity} = \frac{\text{Cov}(x, p)}{s_x s_p}, \quad (1)$$

where p represents the PC, x is a meteorological parameter, and $\text{Cov}(x, p)$ is the covariance, defined by

$$\text{Cov}(x, p) = \frac{1}{M-1} \sum_{i=1}^M [(x_i - \bar{x})(p_i - \bar{p})],$$

where $(x_i - \bar{x})$ and $(p_i - \bar{p})$ represent departures from the ensemble mean of x and p , respectively. The sample standard deviations, s_x and s_p , are defined as

$$s = \left[\frac{1}{M-1} \sum_{i=1}^M (x_i - \bar{x})^2 \right]^{1/2}$$

with the range $1, \dots, M$ representing the ensemble dimension, where $M = 20$. The calculation of Eq. (1) is generated at every grid point over a 20° longitude \times 15° latitude domain surrounding the ensemble cluster, identifying the PC's sensitivity to various meteorological parameters. It is evident that Eq. (1) is simply the Pearson's correlation between the PC and a specific meteorological parameter at every grid point. Caution must be taken when using such a parameter, since nonlinearity between variables is not captured by the correlation. We select meteorological parameters for Eq. (1) that have already been demonstrated to have physical significance with the parameter whose ensemble disagreements were deconstructed via the EOF process. By ensuring the existence of this physical significance, the sensitivities calculated also have physical meaning, even if the relationship is not strictly linear. In this regard, Gombos et al. (2012) explicitly mentioned the dilemma for using model sensitivities to make dynamical inferences about the real atmosphere. Such inferences can only be made when the ensembles realistically represent the true atmospheric state. Since CZM already demonstrated that the ensemble forecasts represent reasonable atmospheric states, dynamical inferences can be made using ensemble sensitivities. Furthermore, keeping consistency with our previous investigations, we preferentially examine MSLP, upper-tropospheric warming, and deep convection to gain a further understanding of their interconnectedness during the TCG of Julia.

4. Dominant ensemble disagreements during the pre-TD stage

At 12 and 6 h before the NHC declared Julia a TD, noteworthy variability (or spread) in several meteorological parameters exists between the ensemble members. This spread is especially pronounced in P_{MIN} estimates, with ensemble sample standard deviation of about 1 hPa at 11/1800 and exceeding 1 hPa at 12/0000. While seemingly small in comparison to ensemble

forecasts spreads for mature tropical cyclones (TCs) or midlatitude disturbances, a spread of 1 hPa could mean the difference between a TD and a nondeveloping tropical disturbance. Thus, it is desirable for us to characterize the MSLP spread into patterns in order to see what "kind" of disagreements exists between the ensemble members. These disagreements may also be isolated in other meteorological parameters, such as upper-tropospheric temperature anomalies and radar reflectivity. Using these isolated patterns of ensemble spread, links between the parameters can be implied, both subjectively and statistically (e.g., through ensemble sensitivity analyses). Furthermore, the evolution of the parametric ensemble spread and associated EOF patterns demonstrate how the pre-TD Julia evolves in the ensemble members and what processes might be responsible for the changes in the patterns of disagreements. In the following subsections, we show the ensemble spreads of MSLP, low-level absolute vorticity, upper-level temperature anomalies, and deep convection, in addition to ensemble sensitivity analyses.

a. Variability in MSLP

Figures 2 and 3 show the ensemble spread, ensemble mean, and the two leading EOFs of MSLP that are identified as the dominant spatial patterns in the ensemble spread at 11/1800 and 12/0000, respectively. We see three regions of heightened spread with respect to the ensemble-mean field at 11/1800. The spread associated with faster-developing ensemble members (or fast developers for short) is marked by "M₁" and symbolizes the creation of pre-TD MSLP disturbances in some members as demonstrated by the cluster of P_{MIN} centers (Fig. 2a). Unlike 11/1800, a bull's-eye of enhanced spread exists at 12/0000, with the sample standard deviation exceeding 1 hPa ("M₁"; Fig. 3a). The overall structure of the ensemble sample standard deviation evolves into a monopole pattern by 12/0000, but with enhanced spread extending eastward back toward the West African coastline ("M₂") in close proximity to M₂ from 11/1800. This eastward spread is supported by the ensemble-mean MSLP, which depicts an elongated closed 1008-hPa isobar extending from the bull's-eye center back to the coastline (Fig. 3a).

The largest mode in the ensemble spread at 11/1800 is depicted by the leading EOF (EOF 1), which explains 29.4% of the variance with a weak monopole pattern centered near M₁ (Fig. 2b). This monopole pattern is a characteristic of an intensity disagreement between the ensemble members as demonstrated in previous studies (Chang et al. 2013; Zheng et al. 2013). Thus, the

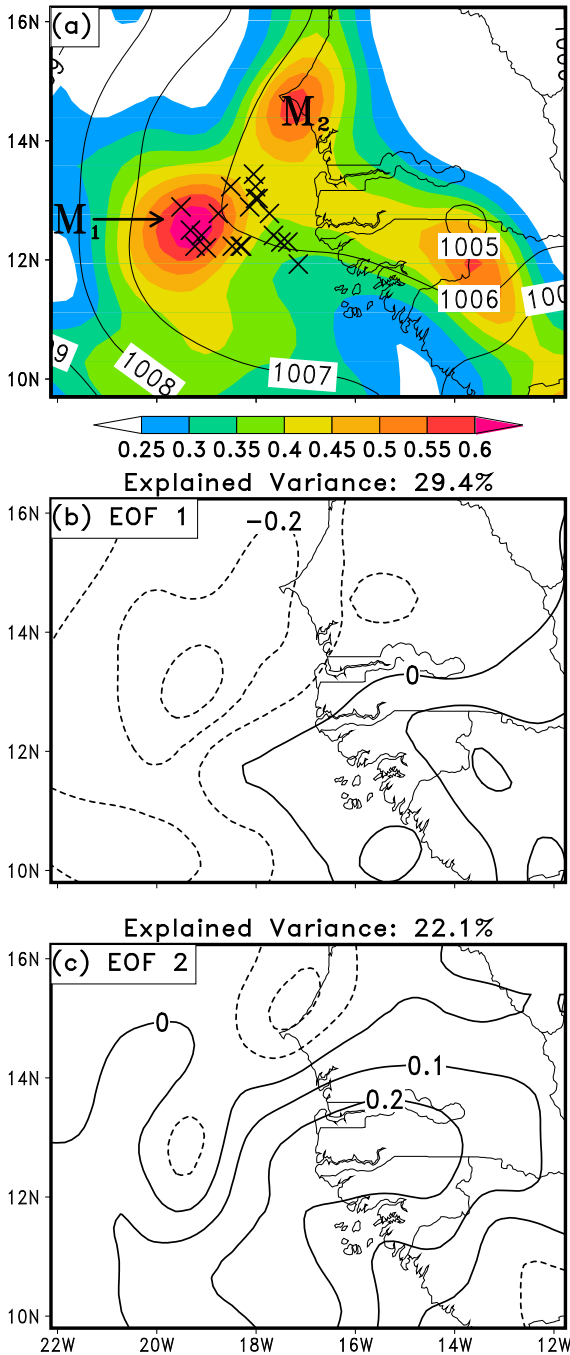


FIG. 2. Spatial distributions, valid at 1800 UTC 11 Sep, of (a) ensemble MSLP standard deviation (shaded, hPa) and ensemble-mean MSLP (contours, interval of 1 hPa), (b) the most reoccurring spatial pattern of MSLP anomalies (i.e., EOF 1) contoured with interval of 0.1 hPa, and (c) the second most reoccurring spatial pattern of MSLP anomalies (EOF 2) contoured with an interval of 0.1 hPa. The explained variance for (b) EOF 1 and (c) EOF 2 are 29.4% and 22.1%, respectively. In (a), “M₁” and “M₂” represent a maximum in the MSLP ensemble spread associated with the faster-developing members and coastal variance, respectively. Each ensemble member’s P_{MIN} center at 1800 UTC 11 Sep is marked by a cross.

pattern of most disagreement between ensemble members at 11/1800 is the intensity of the pre-TD Julia. Since we are looking at the “negative” phase of EOF 1, which happens to represent negative MSLP anomalies, or in other words, ensemble members with positive PC values having stronger pre-TD disturbances at 11/1800. This intensity disagreement becomes increasingly evident at 12/0000 as the leading EOF explains 47.3% of the ensemble spread with a monopole pattern clearly situated within the ensemble cluster and M₁ (Fig. 3b). The leading EOFs from both times are supported by findings from CZM, who depicted intensity differences when assessing the time series of ensemble P_{MIN} disturbances (Fig. 1b). Another common pattern shown previously by Chang et al. (2013) and Zheng et al. (2013) is depicted in the second EOF at 12/0000 (Fig. 3c). This dipole pattern is associated with positional disagreements between the ensemble members, which is consistent with the enhanced spread eastward from the bull’s-eye in Fig. 3a.

It is evident from the EOFs at both times that the most dominant difference between ensemble members is related to the intensity of the pre-TD Julia (Figs. 2b, 3b). As ensemble solutions evolve in time and some members develop pre-TD disturbances in terms of P_{MIN} , the second leading EOF evolves into the positional ensemble differences for the P_{MIN} location (Fig. 3c). Recall that the sign of the EOF pattern is not relevant. Even though EOF 1 represents a stronger storm with negative MSLP anomalies at both times, its sign can be changed to represent the other phase—a weaker storm with positive MSLP anomalies. Moreover, it is worth noting that EOFs can contain more than one pattern (e.g., monopole and dipole), and thus, care needs to be taken to elucidate what possible pattern(s) exists in any given EOF. This being said, since we are dealing with TCG the sign of intensity EOFs will always be chosen so that the positive PC’s represent the stronger storm phase (e.g., negative MSLP anomalies), as we are interested in seeing a stronger TD Julia.

b. Variability in 925-hPa absolute vorticity

Since the growth of the LLV is an important part of TCG (Hendricks et al. 2004; Montgomery et al. 2006; CZ), Fig. 4 shows the 925-hPa absolute vorticity ensemble spread, ensemble mean, and related EOF patterns at 12/0000. At this time, it is expected that a large variability exists between the members, since the process by which the LLV forms is through the merging of numerous mesovortices and enhancement by deep convection. The control-simulated TCG of Julia depicted that two main mesovortices merge just prior to

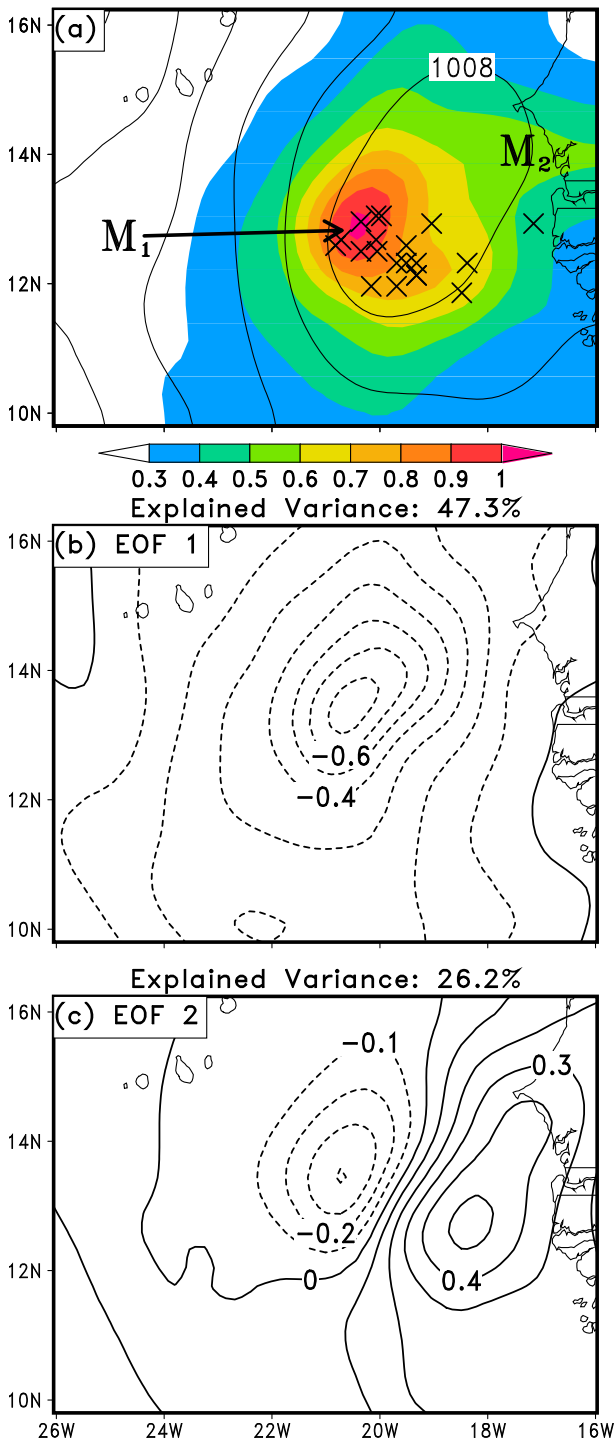


FIG. 3. As in Fig. 2, but valid at 0000 UTC 12 Sep.

and after the TCG time of 12/0600 (CZ). Thus, it is expected that significant ensemble member differences exist for the location and strength of the main mesovortices that become the LLV in each member at 12/0000. These disagreements are in turn expected to

reduce the explained variance for each of the 925-hPa absolute vorticity ensemble-spread EOF patterns.

Similar to the MSLP ensemble spreads at 12/0000, the 925-hPa absolute vorticity spread has two centers of heightened variance: one located over water, the other along on the coastline, marked by “V₁” and “V₂,” respectively (Fig. 4a). The ensemble-mean 925-hPa positive absolute vorticity center exceeds $9 \times 10^{-5} \text{ s}^{-1}$, representing an elongated, weak vortex centered near V₁. Given the weakness of the ensemble-mean vortex with an ensemble spread exceeding $6 \times 10^{-5} \text{ s}^{-1}$ near the ensemble-mean center, it is believed that the mean is averaging through many ensemble member mesovortices near V₁, reducing the positive absolute vorticity magnitude in some areas, while increasing it in the others. The location of the spread near V₂ is similar to that of M₂ in Fig. 3a, though the pattern of vorticity variance is much more pronounced in comparison to its MSLP counterpart.

The leading EOF pattern only explains 22.3% of the variance, representing the low-level vorticity ensemble differences associated near V₁. Comparing the leading EOFs of MSLP and 925-hPa absolute vorticity anomalies (cf. Figs. 3b and 4b), the EOFs are nearly collocated with each other, though the MSLP variance is slightly more westward than the vorticity field. As with EOF 2 of MSLP, EOF 2 of the low-level vorticity field represents a west–east dipole, demonstrating positional disagreements with the developing LLV. Since the first two EOFs explain only 38% of the variance, the third EOF is examined for any meaningful patterns. While much less clear than the leading two EOFs, EOF 3 does hint at intensity uncertainty centered on V₂ and complements the west–east-elongated variance exhibited of MSLP (cf. Figs. 4d and 3a).

c. Variability in upper-tropospheric temperature anomalies

Complementing the disagreements in MSLP and low-level vorticity, similar patterns of ensemble member differences exist for the 400–150-hPa-layer-averaged temperature anomalies shown in Figs. 5 and 6. At 11/1800, three maximum in the upper-tropospheric ensemble spread exist with the spread associated with the fast developers marked by “U₁” (Fig. 5a). The pattern seen in the ensemble spread at 11/1800 has similar characteristics to those of the MSLP ensemble spread, alluding to the two parameters’ variability being linked (cf. Figs. 2a and 5a). These three centers of enhanced upper-tropospheric temperature variance morph into a pattern with two maxima in the ensemble spread at 12/0000: one over water with a magnitude exceeding 0.45°C (“U₁”, Fig. 6a), and the other a slightly weaker

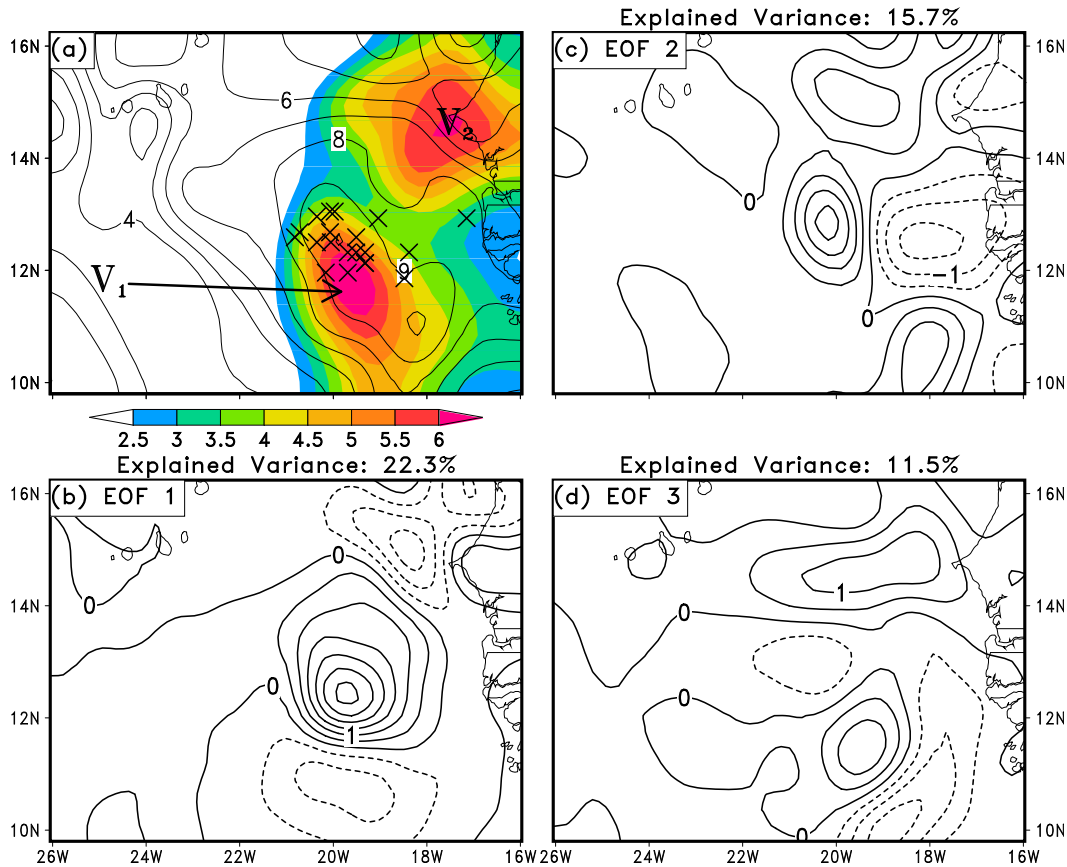


FIG. 4. As in Fig. 2, but for 925-hPa absolute vorticity anomalies ($\times 10^{-5} \text{ s}^{-1}$) valid at 0000 UTC 12 Sep and including (d) EOF 3, which explains 11.5% of the total variance.

maximum near the West African coast with a magnitude of near 0.4°C (“ U_2 ”). As with 11/1800, these two maximums at 12/0000 closely resemble the locations of the two maximum variances in MSLP and low-level vorticity (cf. Figs. 3a, 4a, and 6a), further alluding to some interconnectedness of the parameters. The ensemble spread center at U_1 is collocated with an ensemble-mean warm region with magnitude greater than -41.4°C , while a meso- α area of warming in excess of -41.8°C encompasses both ensemble spread centers (Fig. 6a).

The first EOF pattern of 400–150-hPa temperature anomalies at 11/1800 represents positive temperature anomalies associated the heightened variance near U_1 (Fig. 5b). This pattern explains 28.4% of the variance with a north–south-elongated monopole pattern. The second EOF represents an unbalanced dipole in the north–south direction (Fig. 5c) and explains slightly less variance than EOF 1 but with smaller amplitude compared to the leading EOF (e.g., 0.2° versus 0.15°C). Most importantly, the leading EOF evolves into a monopole representing positive upper-tropospheric

temperature anomalies centered with the enhanced ensemble spread near U_1 at 12/0000 (Fig. 6b). Unlike its counterpart at 11/1800, EOF 2 at 12/0000 represents positive temperature anomalies along the coastline, consistent with the ensemble spread centered near U_2 (cf. Figs. 3c, 4d, and 6c). The enhanced variance associated with EOF 2 can be explained partially by disagreements in deep convection shown in the next subsection.

d. Variability in deep convection anomalies

Previous studies have mentioned the important role of persistent deep convection in TCG through preconditioning the midtroposphere with moisture and its role in upper-tropospheric warming (Dunkerton et al. 2009; Hopsch et al. 2010; CZ; CZM). Thus, it is desirable to evaluate the general convective structure disagreements in the hours prior to TCG. One should keep in mind that substantial variances appear in the location, magnitude, and extent of deep convection during TCG when ensemble member differences are assessed. In this regard, CZM have demonstrated the large differences in

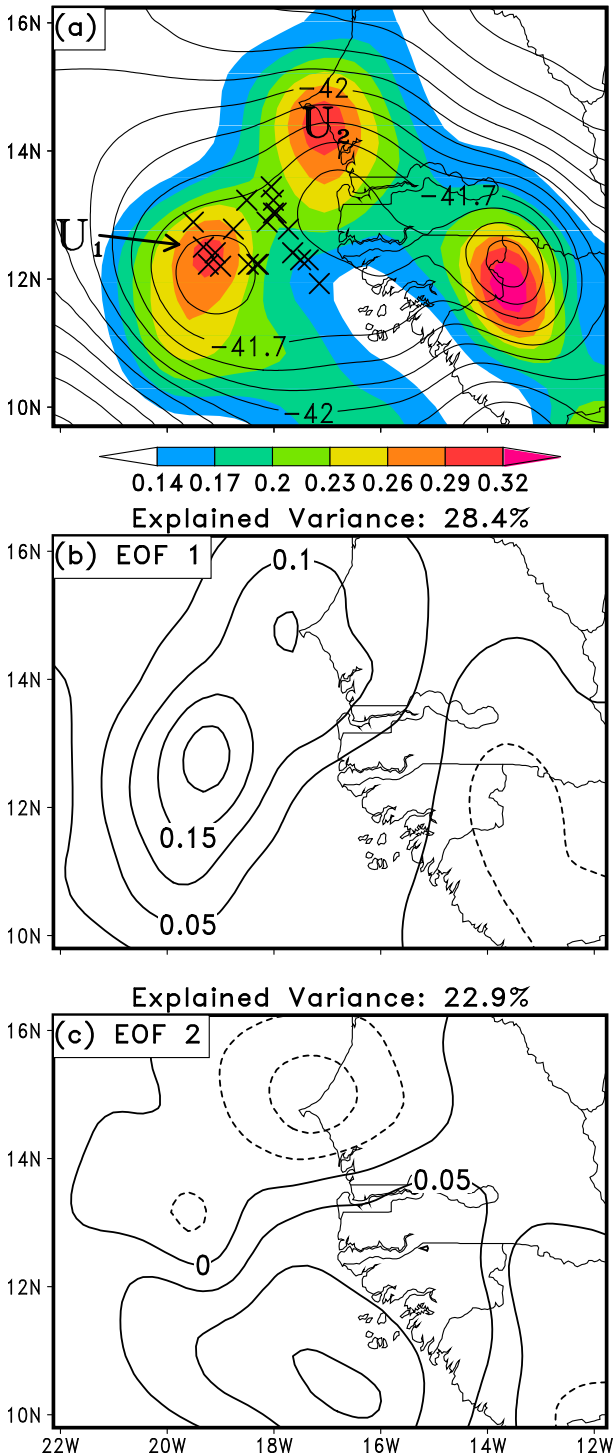


FIG. 5. As in Fig. 2, but for 400–150-hPa-layer-averaged temperature anomalies (°C) valid at 1800 UTC 11 Sep.

deep convection between developers and nondevelopers from the ensemble. As a result, dominant patterns and modes of variability could be much “noisier” than other parameters, such as MSLP.

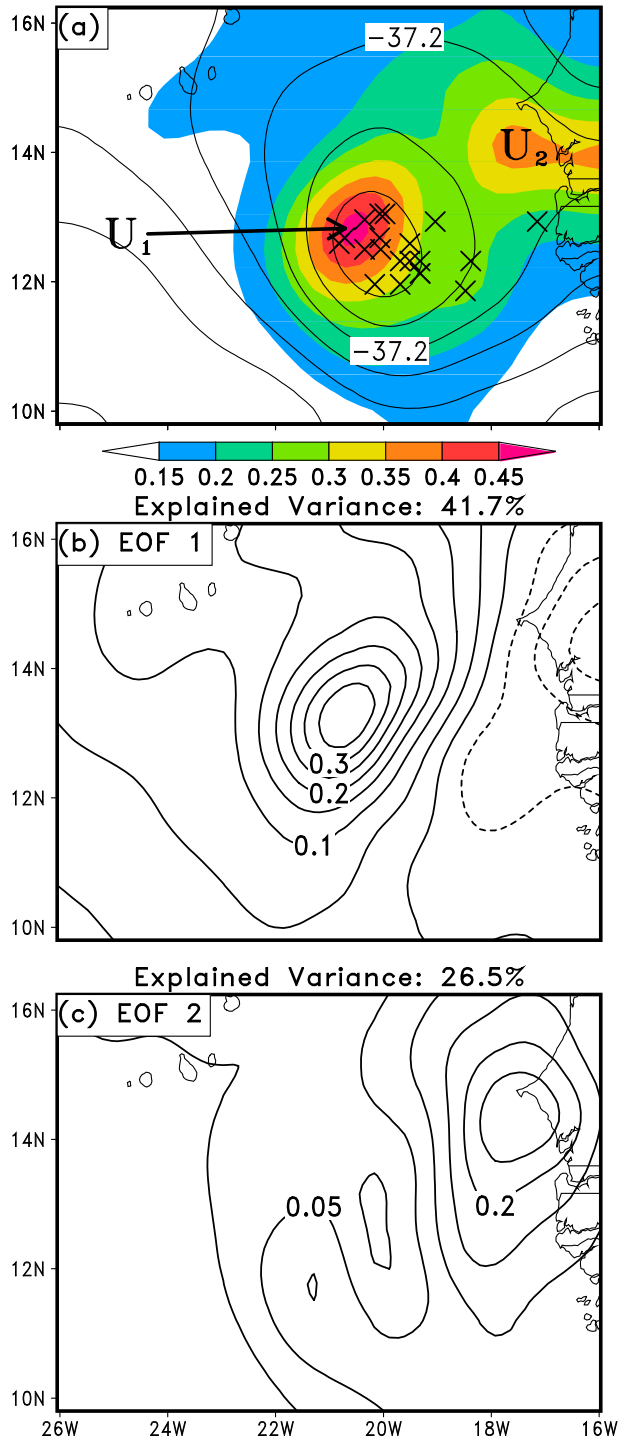


FIG. 6. As in Fig. 2, but for 400–150-hPa-layer-averaged temperature anomalies (°C) valid at 0000 UTC 12 Sep.

At 12/0000, the ensemble spread of composite radar reflectivity exceeds 7 dBZ for an area larger than that encompassed by the ensemble-mean composite radar reflectivity, signifying large disagreements between

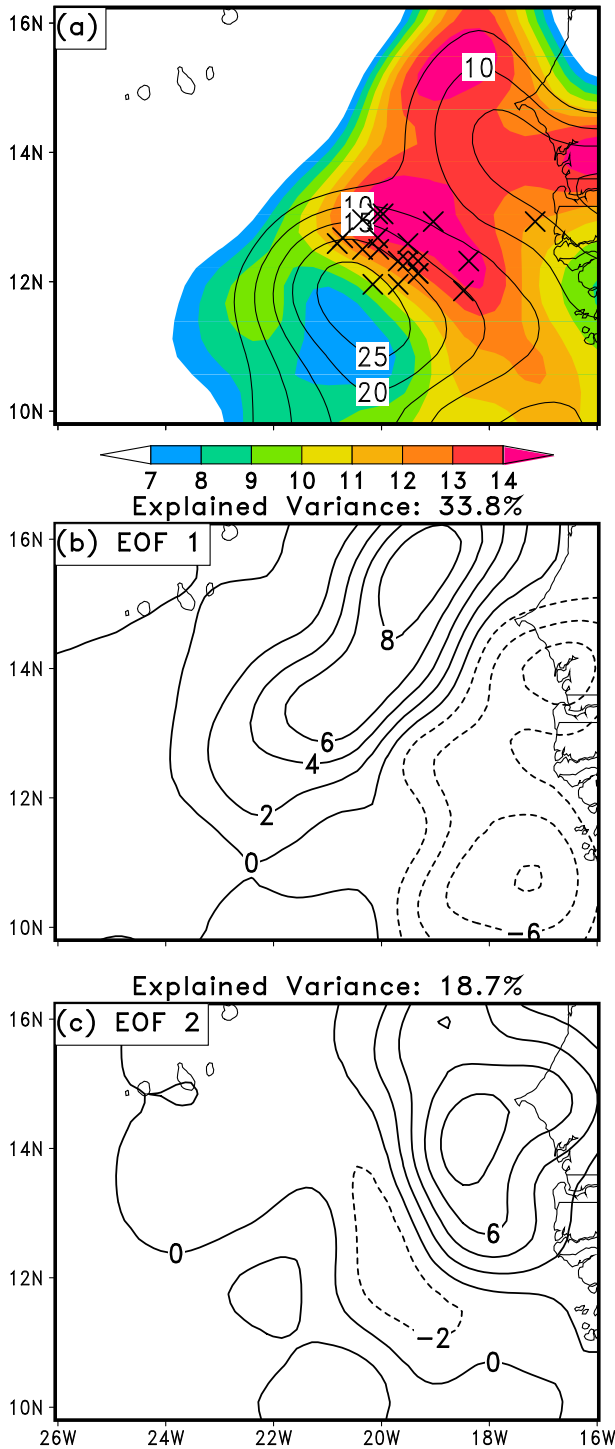


FIG. 7. As in Fig. 2, but for composite radar reflectivity anomalies (dBZ) valid at 0000 UTC 12 Sep.

ensemble members for the placement and intensity of convection associated with the pre-TD disturbance (Fig. 7a). Even with the large variability, the ensemble mean depicts a weak MCS with reflectivity returns

exceeding 25 dBZ centered to the south of the P_{MIN} cluster. Interestingly, the P_{MIN} cluster is closely collocated with ensemble spread exceeding 14 dBZ, hinting at ensemble disagreements with convective development near the storm centers of each member.

Decomposing the ensemble variance reveals two main EOF patterns, explaining 33.8% and 18.7% of the total variance, respectively (Figs. 7b,c). The leading EOF represents a dipole with positive reflectivity anomalies centered to the northeast of the P_{MIN} cluster and ensemble-mean composite radar reflectivity. Such a pattern alludes to the presence of enhanced (or decreased) convection to the north of the ensemble member centers at 12/0000 in addition to positional uncertainties given the location of the gradient of the ensemble-mean reflectivity in relation to the explained variance. The second EOF, however, with its positive composite reflectivity returns over the coastline, closely mimics the location of the second EOF of upper-tropospheric temperature spread (cf. Figs. 6c and 7c), as well as MSLP and low-level positive absolute vorticity (cf. Figs. 3c, 4d, and 7c).

e. Ensemble sensitivity analyses

Given the presence of ensemble disparity in MSLP during pre-TD Julia’s evolution, it is desirable to examine to which parameter(s) these disagreements are sensitive. Both CZ and CZM have demonstrated the importance of upper-tropospheric warming for meso- α -scale MSLP falls during the TCG of Julia. Furthermore, CZM alluded to the importance of deep convection and coherent storm-scale outflow for the development of upper-level warming. To supplement these findings, an ensemble sensitivity analysis with Eq. (1) is used below to identify the mechanisms responsible for the patterns of differences in MSLP and upper-tropospheric temperature anomalies.

1) MSLP 12/0000 EOF 1 SENSITIVITY

Since we are concerned with intensity differences in the forecasts of pre-TD Julia, the PC of EOF 1 of the MSLP variance (Fig. 3b) is used as the forecast metric in Eq. (1), while the 400–150-hPa-layer-averaged temperature anomalies and surface latent heat flux anomalies are employed as the meteorological parameter x to assess the sensitivity of EOF 1. The sensitivity to both parameters is traced back to 11/1200 at a 6-h interval. Given the similarities of the MSLP and low-level vorticity EOF patterns, we decide to choose the MSLP EOFs for sensitivity analyses given our previous research predominately focusing on the MSLP disturbance. Further, CZ showed the formation of a coherent MSLP disturbance on the meso- α scale prior to the existence of a coherent LLV, and obviously, lower MSLPs

enhance PBL convergence, which can enable subsequent growth of the LLV.

As expected, a large positive sensitivity exists between the PC and upper-tropospheric temperature anomalies (Fig. 8a), exceeding 0.6 for the Pearson's correlation. That is, to reproduce the negative MSLP anomalies shown in EOF 1 (Fig. 3b), the upper-tropospheric temperatures must increase accordingly. The cluster of ensemble members whose MSLP minimum are directly collocated with the statistically significant correlations supports the importance of upper-tropospheric temperature anomalies for MSLP falls during TCG as well as the faster developers at 12/0000 (cf. Figs. 3a, 3b, and 8a).

In contrast, the correlation between the PC and surface latent heat flux anomalies is weaker near the peak amplitude of EOF 1, though still reaching statistically significant correlations in collocation with the cluster of ensemble members (Fig. 8d). Much larger correlations with the surface heat flux exist well away from the developing MSLP centers, suggesting stronger winds on the fringes of the developing low-level circulation (Fig. 8d). Given the weakness of the wind speeds of the ensemble at 12/0000, the use of energy from the ocean surface for intensification of the MSLP disturbance is unlikely and, thus, the association can be thought of as substantial variance in the low-level wind speed within the ensemble.

Tracing the sensitivities back in time, it is evident that the upper-tropospheric temperature anomalies at 11/1800 correlate well with the MSLP EOF 1 explained variance at 12/0000 (Fig. 8b). This is contrasted by the surface latent heat flux anomalies whose correlation with the PC quickly diminishes prior to 12/0000 near the ensemble cluster (Figs. 8e,f). This reduction is as expected, however, as prior to 12/0000, the sustained surface winds associated with the pre-TD Julia are mostly below 10 m s^{-1} in all ensemble members and they occur mainly over land (CZM). A stronger correlation to surface latent heat flux anomalies still exists well west from the storm centers, again implying increased winds on the fringes of the developing circulation (Figs. 8e,f). The positive correlation between the upper-tropospheric temperature anomalies and the PC continues at 11/1200 with a slight eastward shift toward the coastline (Fig. 8c).

2) UPPER-TROPOSPHERIC TEMPERATURE 12/0000 EOF 1 SENSITIVITY

Figure 9 shows the sensitivity of the leading EOF of upper-level temperature anomalies to the 400–150-hPa-layer-averaged relative divergence and composite radar reflectivity anomalies. We see that near and to the north of the ensemble cluster center of -36.9°C isotherms strong positive sensitivities occur between the PC of

the leading EOF and 400–150-hPa relative divergence (Fig. 9a). This result indicates that to reproduce EOF 1 and its positive 400–150-hPa-layer-averaged positive temperature anomalies, enhanced divergence in the same layer must occur (e.g., an enhanced storm-scale outflow). This sensitivity near the storm cluster is the largest-magnitude correlation within the domain that the sensitivities are calculated within, suggesting that there is a physical mechanism behind the correlation and, thus, do not represent a “false” sensitivity. In a similar fashion to the relative divergence, strong positive correlations exist between the PC and composite radar reflectivity (Fig. 9d). Such a positive correlation alludes to the need for enhanced convection (positive composite reflectivity anomalies) to reproduce the positive temperature anomalies of EOF 1 (cf. Figs. 6b and 9d). These connections are consistent with CZM, who noted that enhanced deep convection enabled a more coherent storm-scale outflow and, thus, an accumulation of warmth in the upper troposphere as the Rossby radius of deformation shrinks.

At 11/1800, the sensitivity of the upper-tropospheric temperature variance to upper-level divergence and deep convection becomes much less clear. While strong positive correlations between the leading EOF and divergence appear just off the coastline (Fig. 9b), weak correlations, if any, exist farther east near the ensemble cluster. Given that the maximum amplitude of the EOF is purely situated over water, it is believed that the positive correlations seen off the coastline in Fig. 9b do represent the propagation of statistically significant correlations eastward back in time, for example, with the propagation of the convective activity. This is further supported by the physically significant correlations just off the coastline at 11/1200 (Figs. 9c,f), consistent with progression of the AEW and embedded convection off the West African coast.

5. Dominant ensemble differences during the TD stage

As the ensemble solutions evolve, differences between the ensemble members become increasingly evident. A schism between developers and nondevelopers was alluded to in CZM, who demonstrated distinct differences in the ensemble when comparing the MSLP disturbances with upper-tropospheric warming. Even with such a dichotomy, 18 of the 20 ensemble members generate a storm with a P_{MIN} greater than the NHC estimate of 1007 hPa (CZM). Furthermore, the ensemble-mean P_{MIN} of 1004 hPa is 1 hPa stronger than the control simulation. This increase in storm intensity spread coexists with fundamental changes in the spread of upper-tropospheric

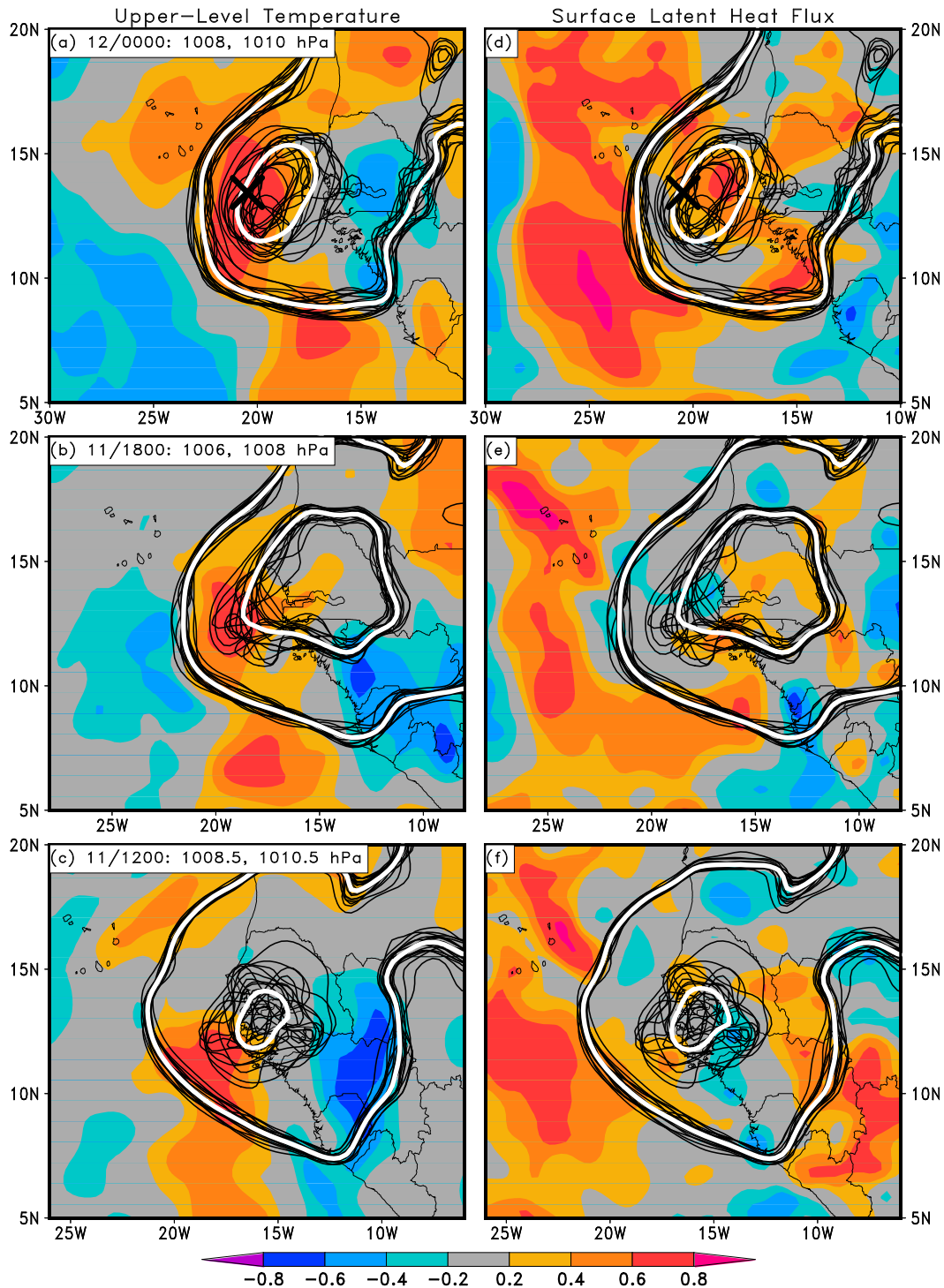


FIG. 8. Ensemble sensitivity [Eq. (1), shaded] of the 0000 UTC 12 Sep MSLP EOF 1 (Fig. 3b) PC values to (a)–(c) the 400–150-hPa-layer-averaged temperature anomalies; and (d)–(f) surface latent heat flux anomalies (± 0.42 is statistically significant at the 95% confidence level). Spaghetti plots for each member’s MSLP (black contours, hPa) and ensemble mean (thick white contour) are overlaid for various isobars. The sensitivities are given at (a),(d) 0000 UTC 12 Sep (i.e., the time at which the EOF pattern is valid), (b),(e) 1800 UTC 11 Sep, and (c),(f) 1200 UTC 11 Sep. The maximum amplitude location of the respective EOF pattern is marked in (a),(d) by a cross.

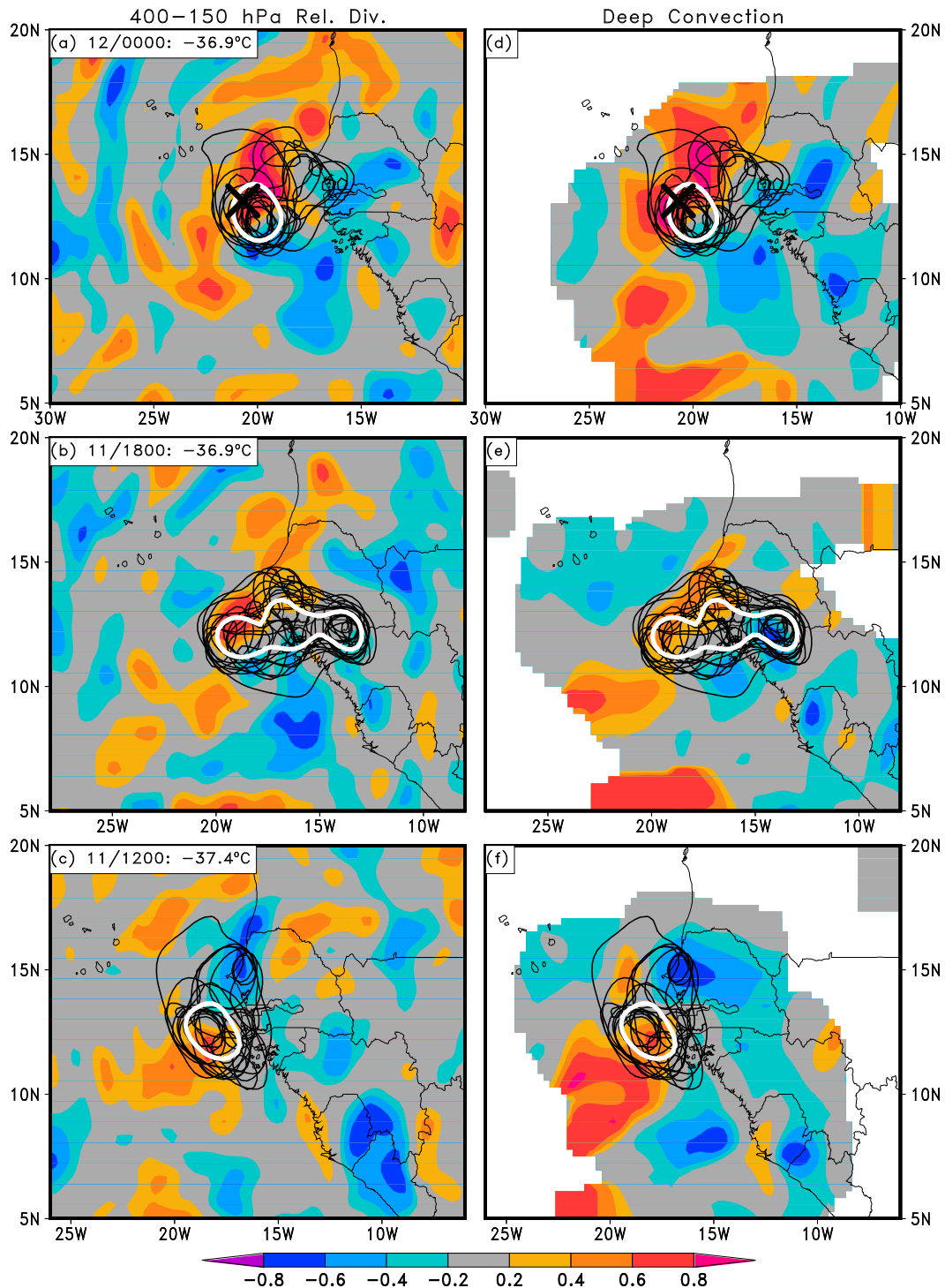


FIG. 9. As in Fig. 8, but for the leading EOF of the 0000 UTC 12 Sep upper-tropospheric temperature anomalies (Fig. 6b) and its sensitivity to (a)–(c) 400–150-hPa-layer-averaged relative divergence anomalies and (d)–(f) the composite radar reflectivity anomalies. The sensitivities depicted in (d)–(f) are only plotted for radar reflectivities greater than 0 dBZ for all ensemble members and the ensemble mean. Otherwise, the sensitivities are masked out since convection does not exist (i.e., composite radar reflectivities at or below 0 dBZ). Spaghetti plots for each member's 400–150-hPa-layer-averaged temperature (black contours, °C) and ensemble mean (thick white contour) are overlaid for various isotherms.

temperatures and meso- α -scale variability in deep convection.

a. Variability in MSLP

The MSLP ensemble spread, ensemble mean, and the leading patterns of spread for 12/0600 are given in Fig. 10, showing that the ensemble spread evolves from its 12/0000 spread pattern into a single monopole (“ M_1 ”) centered near the ensemble mean and the cluster of P_{MIN} centers with little extension back toward the coastline. As expected, the magnitude of ensemble spread further increases from that at 12/0000, demonstrating the divergence of the ensemble member solutions.

As with 12/0000, the leading EOF pattern depicts that the main disagreement between ensemble members is the intensity of the developing Julia (Fig. 10b). However, this pattern only explains 45% of the total spread—a reduction of 2.3% from the similar monopole pattern at 12/0000 (cf. Figs. 10b and 3b). This change is complemented by an increase in variance explained by EOF 2, which portrays a dipole of positional disagreements centered near M_1 with an explained variance of 30.9%. This represents an increase of 4.7% over the positional differences EOF at 12/0000. Even with the change in the amount of total explained variance, the dominant mode of ensemble disagreements between ensemble members regarding TD Julia is storm intensity, followed by northwest–southeast positional disagreements.

b. Variability in 925-hPa absolute vorticity

In a similar fashion to the MSLP variance, the transformation from the two maximum spread centers at 12/0000 to one center at 12/0600 appears in the 925-hPa absolute vorticity as well (“ V_1 ”; Fig. 11a). This spread exceeds $8 \times 10^{-5} s^{-1}$ with the ensemble mean exceeding $12 \times 10^{-5} s^{-1}$ centered on the heightened spread. They represent increases of 2×10^{-5} and $5 \times 10^{-5} s^{-1}$ from their 12/0000 magnitudes, respectively, exemplifying the divergence in ensemble solutions for the development of the LLV. Enhanced ensemble spread extends north of V_1 , suggesting some member disagreements extending to the north of the ensemble cluster. In addition to this northward spread, the maximized spread at V_1 is nearly collocated with the locations of maximum spread of MSLP intensity (cf. Figs. 10a and 11a).

The leading EOF pattern represents east–west positional uncertainties associated with the developing LLV, explaining 27.4% of the variance (Fig. 11b). This pattern is followed by intensity disagreement shown in EOF 2, which has a monopole centered near V_1 and explains 18.1% of the variance. Finally, EOF 3 shows the north–south positional disparity that the ensemble

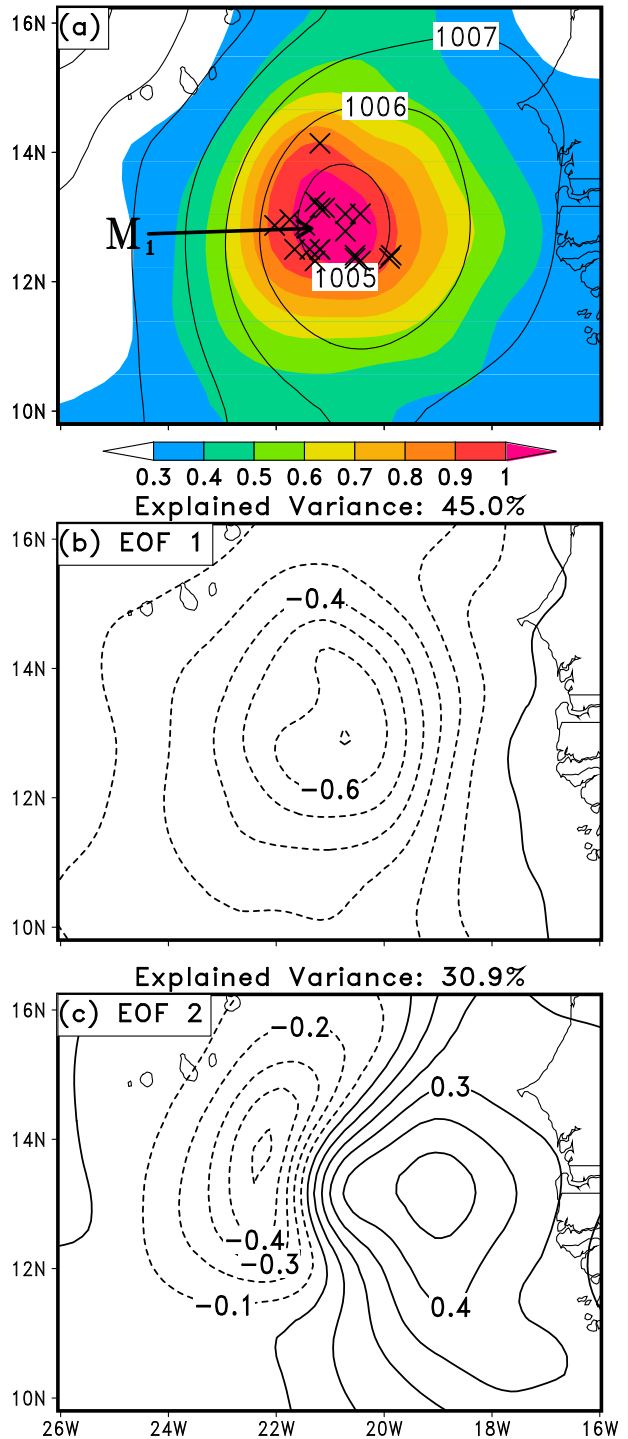


FIG. 10. As in Fig. 2, but valid for 0600 UTC 12 Sep.

spread alluded to (cf. Figs. 11a and 11d). Using these EOF patterns, it is clear that the development of the LLV is underway in the majority of ensemble members with positional and intensity differences that are isolated in the leading EOF patterns.

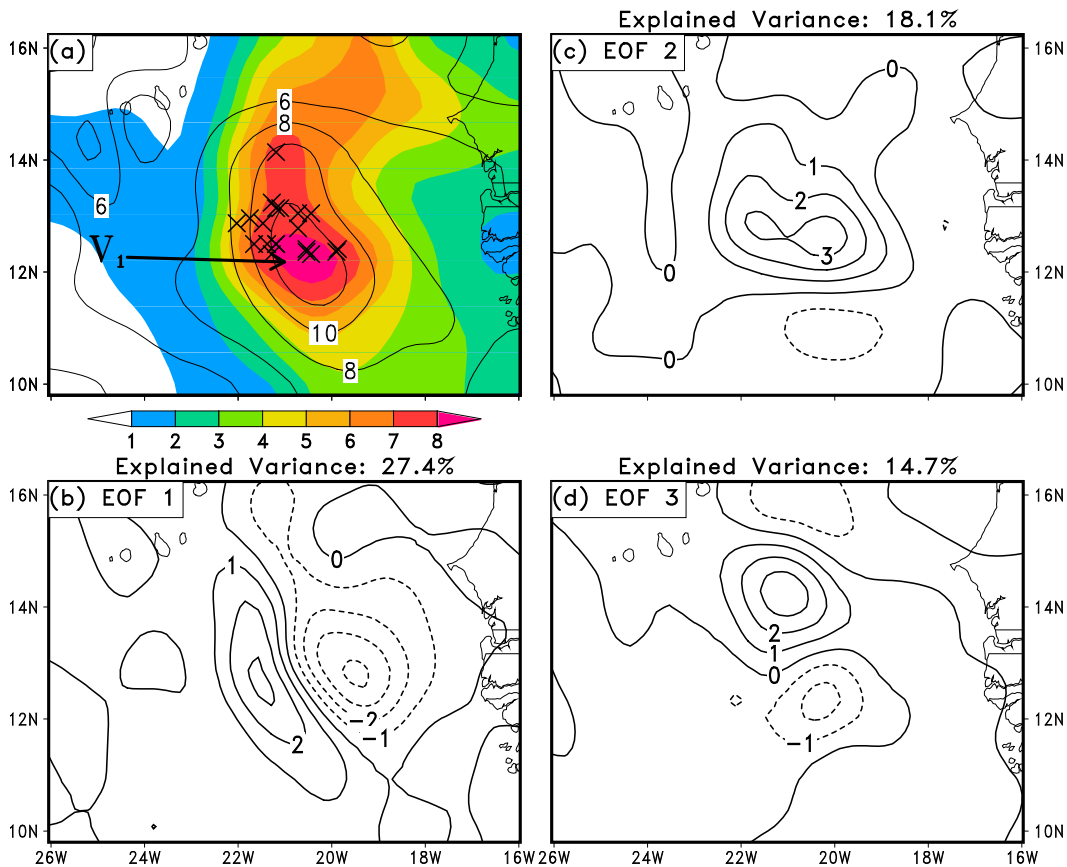


FIG. 11. As in Fig. 2, but for the 925-hPa absolute vorticity ($\times 10^{-5} \text{ s}^{-1}$) valid for 0600 UTC 12 Sep and including (d) EOF 3, which explains 14.7% of the total variance.

c. Variability in upper-tropospheric temperature anomalies

An increase in the upper-tropospheric temperature variability complements the storm intensity disagreements at 12/0600, as shown in Fig. 12a. The ensemble spread of upper-tropospheric temperature exceeds 0.5°C —an increase of 0.05°C from the pre-TD stage (cf. Figs. 6a and 12a). While this increase in spread is notable, the changes to the spatial characteristics of the spread allude to more significant disagreements in the 400–150-hPa-layer-averaged temperature field between ensemble members. Instead of the two maxima seen at 12/0000 (Fig. 6a), a single maximum appears at 12/0600 (see “ U_1 ” in Fig. 12a), suggesting that the main disagreement between the ensemble members is related to the magnitude of the upper-tropospheric temperature anomalies. Additionally, the maximum at U_1 is directly collocated with the maximum ensemble spread of MSLP anomalies (cf. Figs. 10a and 12a) and P_{MIN} cluster, which is consistent with the interconnectedness seen at 12/0000. The ensemble-mean 400–150-hPa-layer-averaged temperatures

show a warming of approximately 0.5°C from 12/0000, with a meso- α -scale region of warmth centered on the ensemble spread (Fig. 12a).

The leading EOF pattern of upper-tropospheric temperature anomalies at 12/0600 describes ensemble differences on the eastern portion of the ensemble cluster, with a monopole pattern displaced just east of the maximum of ensemble spread (Fig. 12b). This pattern explains 42.5% of the total variance, an increase over the 41.7% explained by the leading EOF at 12/0000. EOF 2, explaining 29.2% of the total variance, resembles an uneven dipole with a positive magnitude pole displaced westward of U_1 (Fig. 12c). While technically a dipole, it is clear that EOF 2 resembles more a monopole feature just west of the center of the largest total variance. The superposition of these two EOF patterns represents both the intensity and positional differences associated with the 400–150-hPa-layer-averaged temperature anomalies, with some members displaying an eastward shift in the positive upper-tropospheric temperature anomalies, while others depict a westward shift from the center of maximum total variance. Without the decomposition of

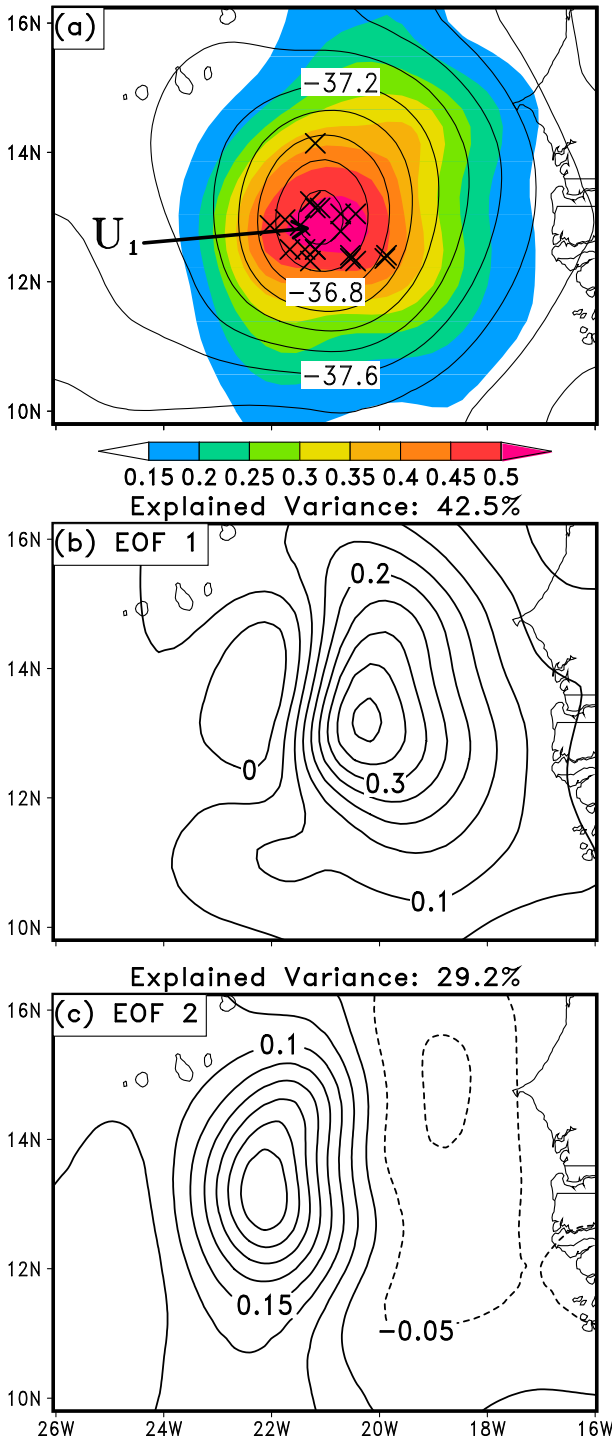


FIG. 12. As in Fig. 2, but for the 400–150-hPa-layer-averaged temperature anomalies ($^{\circ}\text{C}$) valid at 0600 UTC 12 Sep.

the total variance field using EOFs, these characteristics of the ensemble spread would remain unknown, and important features of the ensemble differences would remain overlooked.

d. Variability in deep convection anomalies

As compared to the pre-TD stage, it is evident that the ensemble-mean composite radar reflectivity exhibits a weak MCS with maximum radar reflectivity returns exceeding 30 dBZ, increasing the peak reflectivity by roughly 5 dBZ from 12/0000 (cf. Figs. 7a and 13a). A major difference from 12/0000 is that the ensemble cluster of P_{MIN} is collocated at the center of the ensemble-mean MCS, demonstrating the possibility of substantial convective development near the storm centers of some ensemble members (Fig. 13a). However, in a fashion similar to that at 12/0000, the ensemble spread is maximized to the north of the ensemble-mean center and exceeds 14 dBZ, signifying substantial disagreement between the ensemble members on the northern extent of convective development.

Pulling out the leading EOF yields that the greatest mode of variability between ensemble members for composite radar reflectivity anomalies represents predominantly positional disagreements (Fig. 13b). Even though weak, the uneven magnitude of the dipole depicts that the EOF pattern is not purely positional and includes some intensity differences between ensemble members. EOF 2 depicts intensity disagreement centered on the maximum of ensemble spread with a magnitude exceeding 8 dBZ (Fig. 13c). These two patterns demonstrate that the main ensemble spreads of deep convection are related to the west–east position, as well as the strength of deep convection to the north of the ensemble mean.

e. Ensemble sensitivity analyses

1) MSLP 12/0600 EOF 1 SENSITIVITY

Figure 14 presents the ensemble sensitivity analysis for PC 1 of MSLP anomalies (Fig. 10b). The instantaneous sensitivity (Figs. 14a,d) is strongly positive near the 1006-hPa ensemble cluster with correlations exceeding 0.8 for both parameters. A notable increase from 12/0000 in the instantaneous sensitivity between the PC and surface latent heat flux anomalies occurs with correlations exceeding 0.6 for the majority of the ensemble cluster. This is further evidenced by the substantially larger region of statistically significant correlations, alluding to the increase in intensity and spatial extent of the low-level circulation field as exemplified 1009-hPa ensemble cluster (Fig. 14d). The strongest correlations between the PC and upper-tropospheric temperature exist to the southwest of the ensemble cluster, suggesting enhanced MSLP variance resulting from the upper-tropospheric temperatures downstream of the greatest MSLP variance (Fig. 14a). The ensemble-mean

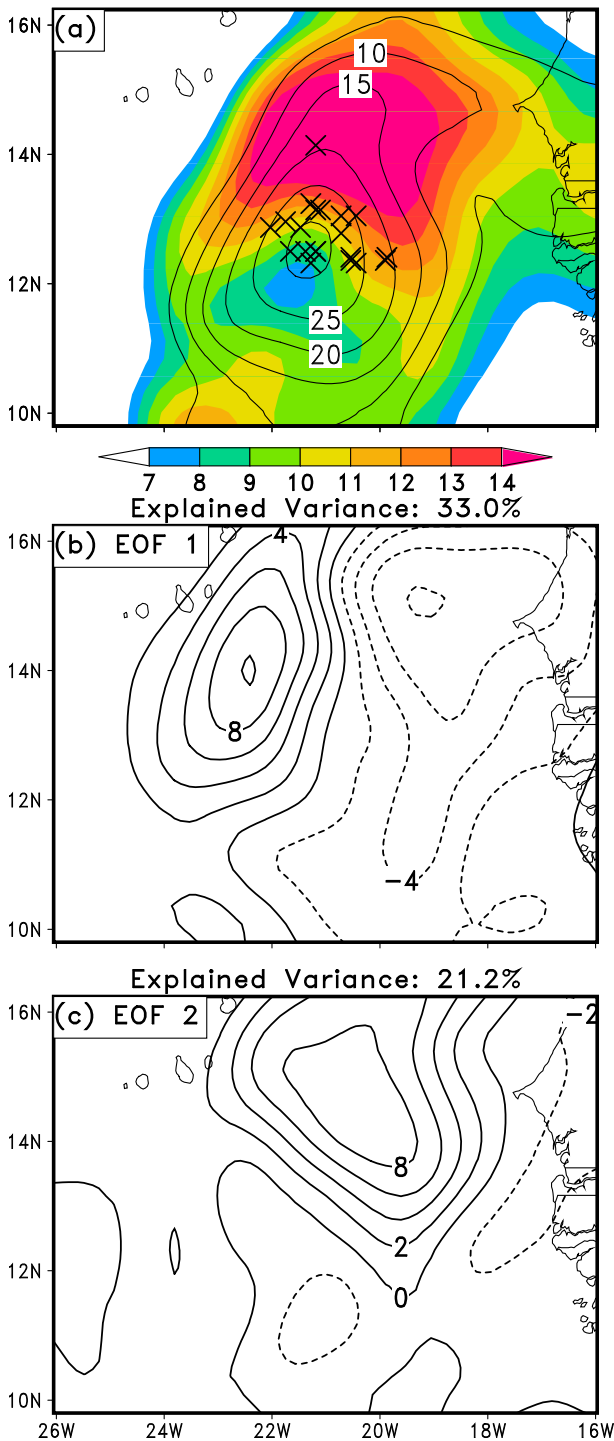


FIG. 13. As in Fig. 2, but for the composite radar reflectivity anomalies (dBZ) valid at 0600 UTC 12 Sep.

surface maximum wind exceeds 12 m s^{-1} and, thus, wind-induced surface heat exchange (WISHE; Emanuel et al. 1994) can be utilized for generating MSLP falls in the stronger ensemble members. Since PC 1 is strongly

correlated with both parameters within the ensemble cluster at 12/0600, we may state that both hydrostatically induced and WISHE-induced MSLP falls are occurring and are dependent on the strength of the ensemble member disturbance.

Tracing the sensitivities back in time, statistically significant positive correlations between PC 1 and upper-tropospheric temperature anomalies exist back until 11/1800 near the ensemble cluster and within the general larger-scale disturbance encompassed by the 1010-hPa isobar cluster at 12/0000 (Figs. 14b,c). On the other hand, the positive correlations between PC 1 and surface latent heat flux anomalies diminish quickly, with an indiscernible correlation at 11/1800 (Figs. 14e,f). The most notable reduction of statistically significant positive correlation exists between 12/0600 and 12/0000 as the most robust correlations are confined to the edges of the developing low-level circulation (Fig. 14e). Some statistically significant correlations exist with the latent heat flux anomalies near the ensemble cluster but are much less meaningful when compared to the upper-tropospheric temperatures (cf. Figs. 14b and 14e). The reduction in correlations with surface latent heat flux anomalies makes physical sense, however, as the ensemble-mean surface maximum sustained wind speed is below 10 m s^{-1} at 11/1800 (CZM) and, thus, the MSLP variance at 12/0600 is unlikely to be caused by positive surface latent heat flux anomalies at 11/1800.

2) UPPER-TROPOSPHERIC TEMPERATURE 12/0600 EOF 1 AND 2 SENSITIVITIES

Since both EOFs patterns depicted in Figs. 12b and 12c represent important features of the upper-temperature ensemble spread, it is of interest to examine the sensitivity of both EOFs to the 400–150-hPa-layer-averaged relative divergence and composite radar reflectivity anomalies.

Figure 15 shows the sensitivity of EOF 1 to upper-level divergence and deep convection. As at 12/0000, a strong positive instantaneous sensitivity exists between the PC of the EOF and both meteorological parameters near the ensemble cluster and maximum amplitude of the EOF pattern (see the crosses in Figs. 15a and 15d). These positive sensitivities shift eastward back in time as the upper-tropospheric temperatures at 12/0600 are well correlated with enhanced deep convection and divergence propagating off the West African coastline. Similar patterns and correlations are seen for the second EOF (Fig. 12c) with relevant positive correlations with divergence and composite radar reflectivity anomalies near the ensemble cluster and maximum-amplitude location of the EOF (Fig. 16).

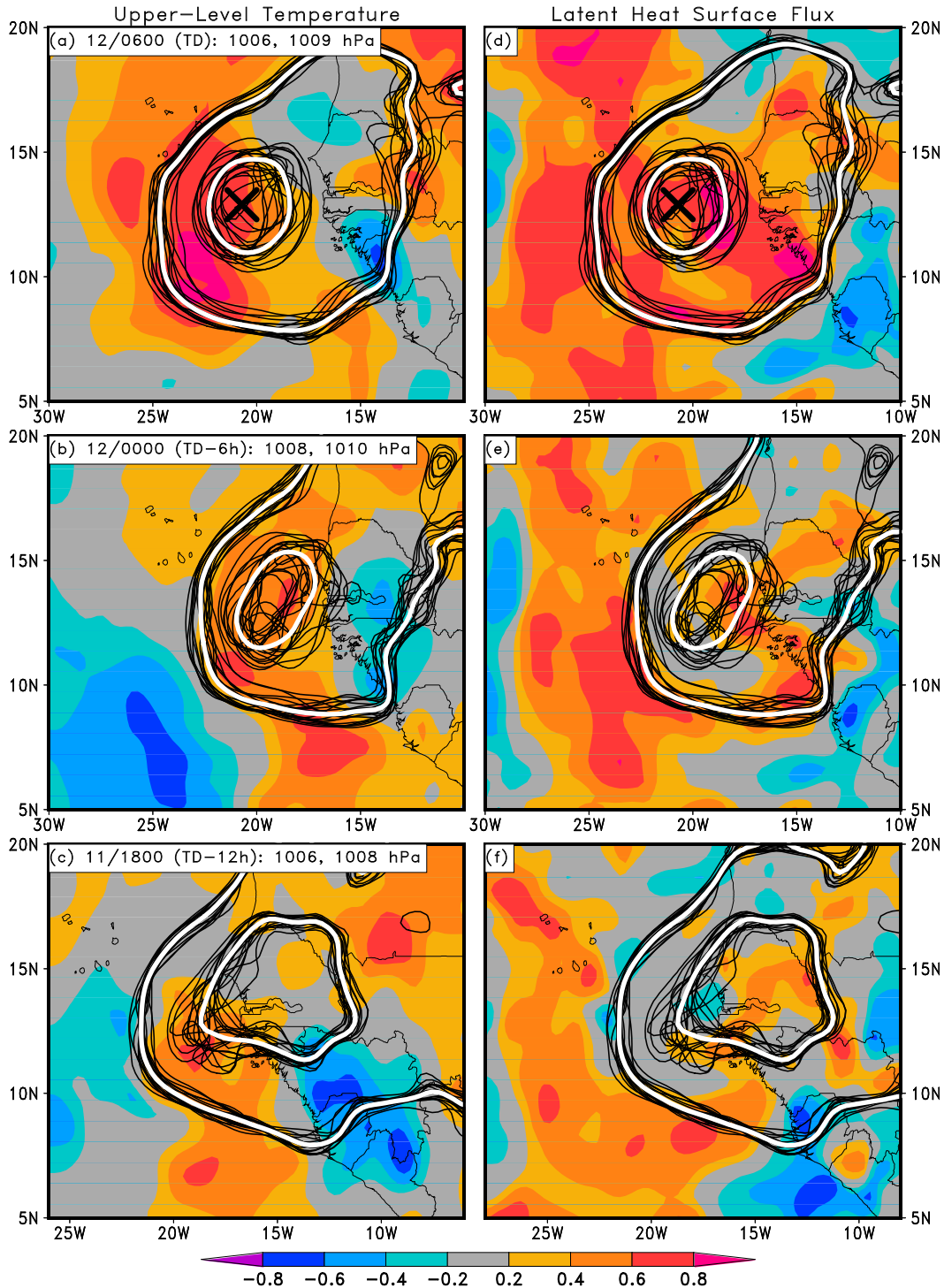


FIG. 14. As in Fig. 8, but for the sensitivity of the 0600 UTC 12 Sep MSLP EOF 1 (Fig. 10b) PC values.

While other sensitivities exist for both EOFs away from the ensemble clusters, they are generally of less magnitude than those of the sensitivities near the cluster and, thus, yield little, if any, meaningful information on the implications for the EOF patterns examined.

6. Summary and final thoughts

In this study, we constructed EOFs for multiple parameters to identify the dominant patterns of ensemble spreads for the TCG of Hurricane Julia (2010). Using

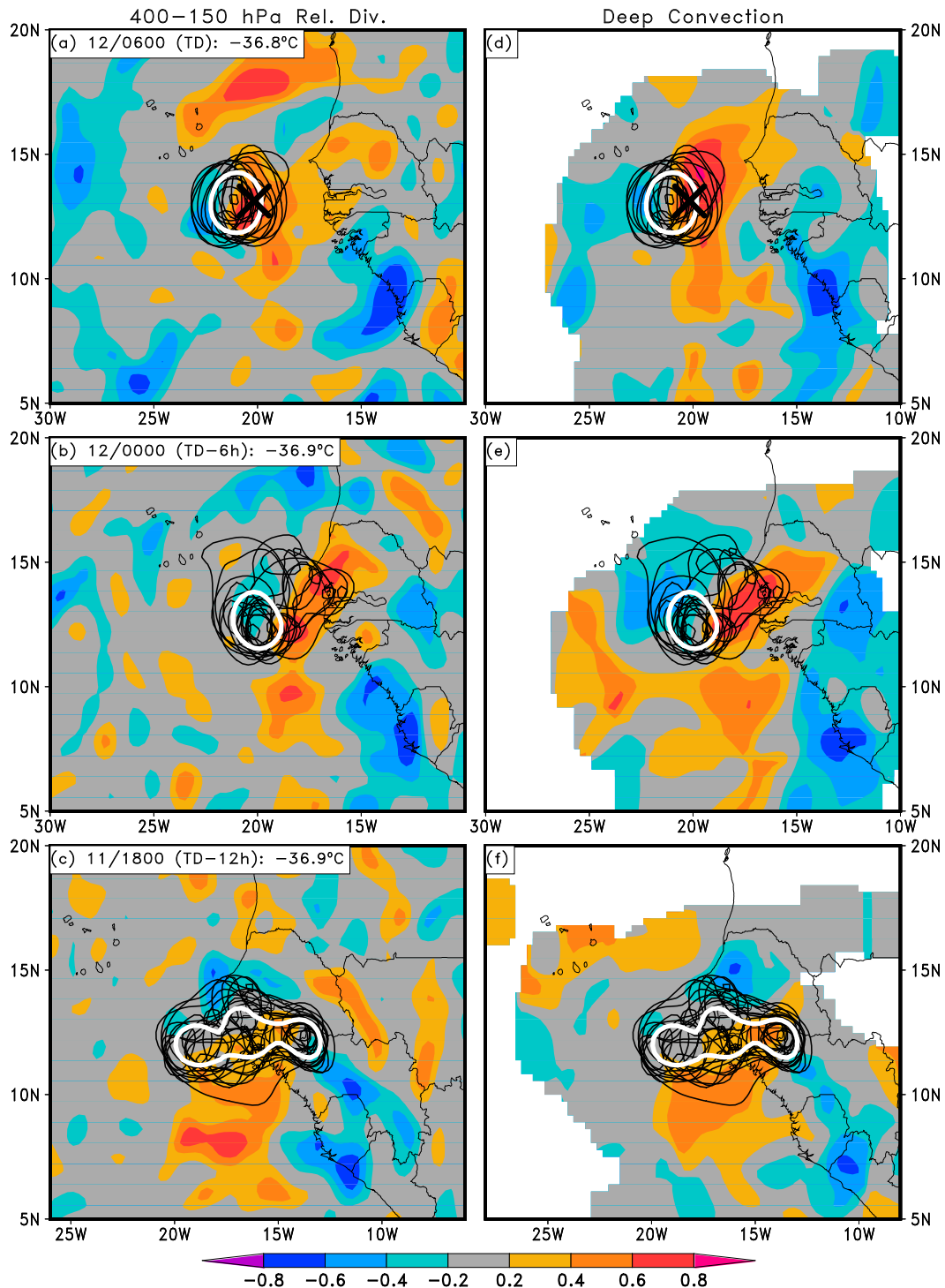


FIG. 15. As in Fig. 9, but for the sensitivity of the 0600 UTC 12 Sep upper-tropospheric temperature EOF 1 PC values (Fig. 12b).

these parametric patterns of differences, we are able to make inferences for the dominant mechanisms responsible for the ensemble spreads and for how each of the spread of the multiple parameters is connected. Two

main stages were investigated for parametric ensemble differences: (i) pre-TD stage and (ii) TD stage.

It is found that the dominant pattern of MSLP disagreements is related to the intensity of the pre-TD and

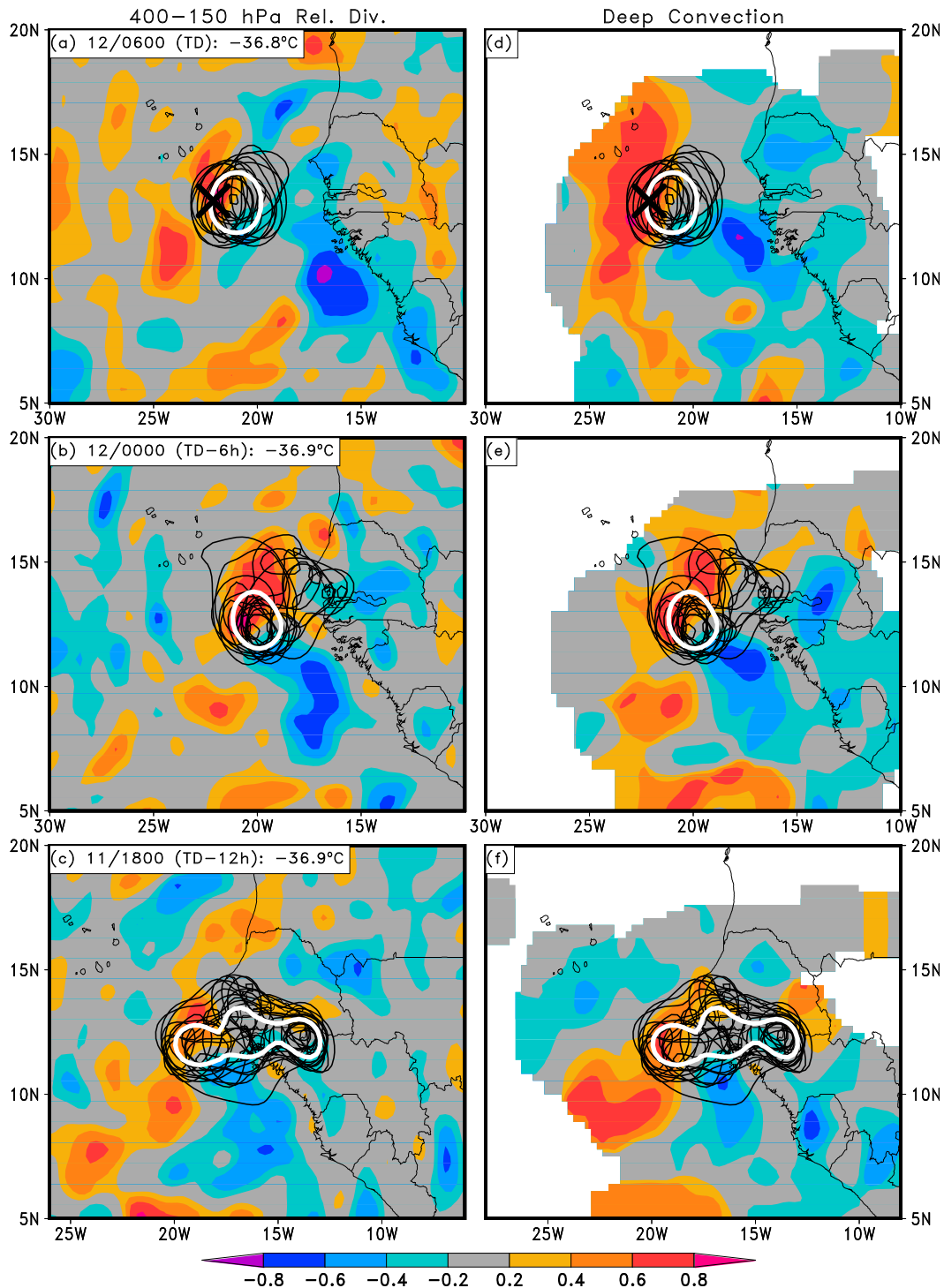


FIG. 16. As in Fig. 9, but for the sensitivity of the 0600 UTC 12 Sep upper-tropospheric temperature EOF 2 PC values (Fig. 12c).

TD Julia, explaining nearly half of the total ensemble variance at both times. The second leading mode of variance for MSLP is related to the position of the developing TD Julia, demonstrating the difference

between faster- and slower-developing members. Similar patterns are found in the variance of 925-hPa absolute vorticity, though with much less explained variance per EOF.

The ensemble spread in MSLP and low-level absolute vorticity is complemented by similar patterns of variance in upper-tropospheric temperatures, suggesting that the variances of the variables are linked. At the pre-TD stage, the maximum of multiple MSLP variance centers are collocated with centers of the maximum upper-tropospheric temperature variance. As the MSLP variance pattern morphs into a monopole pattern during the TD stage, so does the upper-level temperature variance, closely located to the cluster of ensemble-member storm centers. Consistent with the pre-TD stage, the EOFs at the TD stage depict the same characteristics but characteristic patterns representing faster- and slower-developing members, instead of just one group of ensemble members.

To examine what causes the MSLP changes during TCG, ensemble sensitivity analyses were performed to compare if upper-tropospheric temperature anomalies or surface latent heat flux anomalies (i.e., extracting energy from the ocean surface) are responsible for the MSLP changes at both stages. At the pre-TD stage, strong positive sensitivities exist between the upper-tropospheric temperature anomalies and the EOF representing negative MSLP anomalies (e.g., a stronger pre-TD Julia). This sensitivity is coherent and traceable back in time, suggesting that to make the pre-TD Julia stronger, increases in upper-tropospheric temperatures must occur in the hours prior and at 12/0000. Contrasting this result, the sensitivity of the EOF pattern to surface latent heat flux anomalies at the pre-TD stage is less robust. While some positive correlation exists instantaneously, the sensitivity quickly diminishes back in time. Links between upper-tropospheric temperature anomalies and deep convection are illustrated through further ensemble sensitivity analyses. It is evident that the strength of the upper-level warming during TCG is positively correlated to enhanced composite radar reflectivity anomalies (e.g., enhanced deep convection) and its divergent outflow.

Overall, the results herein paint a more holistic picture describing the predictability of TCG of Hurricane Julia through a variety of statistical inferences of important meteorological parameters for the occurrence of TCG. The methods herein would benefit other studies using ensembles to investigate particular meteorological phenomena, including TCs. Identifying the dominant characteristics of the ensemble as a whole can provide a much more robust analysis than investigating and comparing individual ensemble members. That being said, the method does have its deficiencies, mainly that statistical inferences of dynamical processes can yield unrealistic conclusions or ones that do not adhere to the governing equations. Regardless of this shortcoming,

the results presented herein provide insight on the dominant modes of variability occurring during TCG and elucidate how the variability of multiple parameters is woven together.

Acknowledgments. This work was supported by NASA Headquarters under the NASA Earth and Space Science Fellowship Program Grant NNX11AP29H and NASA's Grant NNX12AJ78G. Model simulations were performed at the NASA High-End Computing (HEC) Program through the NASA Center for Climate Simulation (NCCS) at Goddard Space Flight Center.

REFERENCES

- Ancell, B., and G. J. Hakim, 2007: Comparing adjoint- and ensemble-sensitivity analysis with applications to observation targeting. *Mon. Wea. Rev.*, **135**, 4117–4134, doi:10.1175/2007MWR1904.1.
- Braun, S. A., and Coauthors, 2013: NASA's Genesis and Rapid Intensification Processes (GRIP) field experiment. *Bull. Amer. Meteor. Soc.*, **94**, 345–363, doi:10.1175/BAMS-D-11-00232.1.
- Cecelski, S. F., and D.-L. Zhang, 2013: Genesis of Hurricane Julia (2010) within an African easterly wave: Low-level vortices and upper-level warming. *J. Atmos. Sci.*, **70**, 3799–3817, doi:10.1175/JAS-D-13-043.1.
- , —, and T. Miyoshi, 2014: Genesis of Hurricane Julia (2010) within an African easterly wave: Developing and non-developing members from WRF-LETKF ensemble forecasts. *J. Atmos. Sci.*, **71**, 2763–2781, doi:10.1175/JAS-D-13-0187.1.
- Chang, E. K. M., M. Zheng, and K. Raeder, 2013: Medium-range ensemble sensitivity analysis of two extreme Pacific extratropical cyclones. *Mon. Wea. Rev.*, **141**, 211–231, doi:10.1175/MWR-D-11-00304.1.
- Dunkerton, T. J., M. T. Montgomery, and Z. Wang, 2009: Tropical cyclogenesis in a tropical wave critical layer: Easterly waves. *Atmos. Chem. Phys.*, **9**, 5587–5646, doi:10.5194/acp-9-5587-2009.
- Emanuel, K. A., J. D. Neelin, and C. S. Bretherton, 1994: On large-scale circulations in convecting atmospheres. *Quart. J. Roy. Meteor. Soc.*, **120**, 1111–1144, doi:10.1002/qj.49712051902.
- Gombos, D., R. N. Hoffman, and J. A. Hansen, 2012: Ensemble statistics for diagnosing dynamics: Tropical cyclone track forecast sensitivities revealed by ensemble regression. *Mon. Wea. Rev.*, **140**, 2647–2669, doi:10.1175/MWR-D-11-00002.1.
- Hawblitzel, D. P., F. Zhang, Z. Meng, and C. A. Davis, 2007: Probabilistic evaluation of the dynamics and predictability of the mesoscale convective vortex of 10–13 June 2003. *Mon. Wea. Rev.*, **135**, 1544–1563, doi:10.1175/MWR3346.1.
- Hendricks, E. A., M. T. Montgomery, and C. A. Davis, 2004: The role of “vortical” hot towers in the formation of Tropical Cyclone Diana (1984). *J. Atmos. Sci.*, **61**, 1209–1232, doi:10.1175/1520-0469(2004)061<1209:TROVHT>2.0.CO;2.
- Hopsch, S. B., C. D. Thorncroft, and K. R. Tyle, 2010: Analysis of African easterly wave structures and their role in influencing tropical cyclogenesis. *Mon. Wea. Rev.*, **138**, 1399–1419, doi:10.1175/2009MWR2760.1.
- Houze, R. A., W.-C. Lee, and M. M. Bell, 2009: Convective contribution to the genesis of Hurricane Ophelia (2005). *Mon. Wea. Rev.*, **137**, 2778–2800, doi:10.1175/2009MWR2727.1.
- Hunt, B. R., E. J. Kostelich, and I. Szunyogh, 2007: Efficient data assimilation for spatiotemporal chaos: A local ensemble

- transform Kalman filter. *Physica D*, **230**, 112–126, doi:10.1016/j.physd.2006.11.008.
- Miyoshi, T., and M. Kunii, 2012: The local ensemble transform Kalman filter with the weather research and forecasting model: Experiments with real observations. *Pure Appl. Geophys.*, **169**, 321–333, doi:10.1007/s00024-011-0373-4.
- Montgomery, M. T., M. E. Nicholls, T. A. Cram, and A. B. Saunders, 2006: A vortical hot tower route to tropical cyclogenesis. *J. Atmos. Sci.*, **63**, 355–386, doi:10.1175/JAS3604.1.
- , L. L. Lussier III, R. W. Moore, and Z. Wang, 2010: The genesis of Typhoon Nuri as observed during the Tropical Cyclone Structure 2008 (TCS-08) field experiment—Part 1: The role of the easterly wave critical layer. *Atmos. Chem. Phys.*, **10**, 9879–9900, doi:10.5194/acp-10-9879-2010.
- , and Coauthors, 2012: The Pre-Depression Investigation of Cloud-Systems in the Tropics (PREDICT) experiment: Scientific basis, new analysis tools, and some first results. *Bull. Amer. Meteor. Soc.*, **93**, 153–172, doi:10.1175/BAMS-D-11-00046.1.
- Sippel, J. A., and F. Zhang, 2008: A probabilistic analysis of the dynamics and predictability of tropical cyclogenesis. *J. Atmos. Sci.*, **65**, 3440–3459, doi:10.1175/2008JAS2597.1.
- , J. W. Nielsen-Gammon, and S. E. Allen, 2006: The multiple-vortex nature of tropical cyclogenesis. *Mon. Wea. Rev.*, **134**, 1796–1814, doi:10.1175/MWR3165.1.
- Torn, R. D., and G. J. Hakim, 2008: Ensemble-based sensitivity analysis. *Mon. Wea. Rev.*, **136**, 663–677, doi:10.1175/2007MWR2132.1.
- , and D. Cook, 2013: The role of vortex and environment errors in genesis forecasts of Hurricanes Danielle and Karl (2010). *Mon. Wea. Rev.*, **141**, 232–251, doi:10.1175/MWR-D-12-00086.1.
- Wang, Z., M. T. Montgomery, and T. J. Dunkerton, 2010: Genesis of pre-Hurricane Felix (2007). Part I: The role of the easterly wave critical layer. *J. Atmos. Sci.*, **67**, 1711–1729, doi:10.1175/2009JAS3420.1.
- Zhang, D.-L., and L. Zhu, 2012: Roles of upper-level processes in tropical cyclogenesis. *Geophys. Res. Lett.*, **39**, L17804, doi:10.1029/2012GL053140.
- Zheng, M., E. K. M. Chang, and B. A. Colle, 2013: Ensemble sensitivity tools for assessing extratropical cyclone intensity and track predictability. *Wea. Forecasting*, **28**, 1133–1156, doi:10.1175/WAF-D-12-00132.1.